https://doi.org/10.1038/s41591-021-01332-7

nature medicine

# Transcriptional analysis of cystic fibrosis airways at single-cell resolution reveals altered epithelial cell states and composition

Gianni Carraro[1,14], Justin Langerman[2,14], Shan Sabri[2], Zareeb Lorenzana[3,4], Arunima Purkayastha[5], Guangzhu Zhang[1], Bindu Konda[1], Cody J. Aros[5,6,7], Ben A. Calvert[3], Aleks Szymaniak[8], Emily Wilson[8], Michael Mulligan[8], Priyanka Bhatt[8], Junjie Lu[8], Preethi Vijayaraj[5], Changfu Yao[1], David W. Shia[5,6,7], Andrew J. Lund[5,6], Edo Israely[1], Tammy M. Rickabaugh[5], Jason Ernst[2,9,10], Martin Mense[8], Scott H. Randell[11], Eszter K. Vladar[12], Amy L. Ryan[3,4], Kathrin Plath[2,9,10,15] ✉, John E. Mahoney[8,15] ✉, Barry R. Stripp[1,15] ✉ and Brigitte N. Gomperts[5,9,10,13,15] ✉

**Cystic fibrosis (CF) is a lethal autosomal recessive disorder that afflicts more than 70,000 people. People with CF experience multi-organ dysfunction resulting from aberrant electrolyte transport across polarized epithelia due to mutations in the cystic fibrosis transmembrane conductance regulator (*CFTR*) gene. CF-related lung disease is by far the most important determinant of morbidity and mortality. Here we report results from a multi-institute consortium in which single-cell transcriptomics were applied to define disease-related changes by comparing the proximal airway of CF donors ($n=19$) undergoing transplantation for end-stage lung disease with that of previously healthy lung donors ($n=19$). Disease-dependent differences observed include an overabundance of epithelial cells transitioning to specialized ciliated and secretory cell subsets coupled with an unexpected decrease in cycling basal cells. Our study yields a molecular atlas of the proximal airway epithelium that will provide insights for the development of new targeted therapies for CF airway disease.**

## Transcriptome of single cells from control and CF airways

There is great interest in defining human bronchial epithelial (hBE) cell subsets in normal and CF airways to aid development of gene therapeutic strategies for long-term correction of *CFTR* function[1–3]. To address this, we produced single-cell reference atlases of proximal airway epithelium isolated from donors with no evidence of chronic lung disease (referred to as control (CO) samples; $n=19$) compared to explant tissue from patients undergoing transplantation for end-stage CF lung disease (referred to as CF samples, $n=19$) (Supplementary Table 1). Single cells were isolated from proximal airways at three institutions (Fig. 1a), using similar yet distinct methodologies (Fig. 1b and Methods), and datasets were integrated for subsequent analyses. Although cells from each institution were homogeneously integrated, expression of some genes, particularly those associated with metabolic state, showed differential expression by institution (Extended Data Fig. 1a–f). Accordingly, only data that were reproducibly observed across each of the three institutions were highlighted in this study.

Uniform manifold approximation and projections (UMAPs) comparing cells from CO versus CF samples revealed a high degree of overlap (Fig. 1c). Using cell type gene signatures from Plasschaert et al.[1], we identified all major human airway epithelial cell types, including basal, secretory and ciliated, in addition to rare cell types, including ionocytes, neuroendocrine (NE) and *FOXN4*$^{+}$ cell populations (Extended Data Fig. 1g,h). We then performed differentially expressed gene (DEG) analysis between clusters to discern cell subsets with unique molecular characteristics. Among the three major cell types, we were able to resolve three ciliated, five secretory and five basal cell subsets (Fig. 1c and Supplementary Table 2). These subsets were found in similar proportions in CO and CF samples or between institutions (Fig. 1d and Extended Data Fig. 1i).

[1]Lung and Regenerative Medicine Institutes, Department of Medicine, Cedars-Sinai Medical Center, Los Angeles, CA, USA. [2]Department of Biological Chemistry, David Geffen School of Medicine, University of California, Los Angeles, Los Angeles, CA, USA. [3]Hastings Center for Pulmonary Research and Division of Pulmonary, Critical Care and Sleep Medicine, Department of Medicine, Keck School of Medicine, University of Southern California, Los Angeles, CA, USA. [4]Department of Stem Cell Biology and Regenerative Medicine, Keck School of Medicine, University of Southern California, Los Angeles, CA, USA. [5]UCLA Children's Discovery and Innovation Institute, Mattel Children's Hospital UCLA, Department of Pediatrics, David Geffen School of Medicine, University of California, Los Angeles, Los Angeles, CA, USA. [6]Department of Molecular Biology Interdepartmental Program, University of California, Los Angeles, Los Angeles, CA, USA. [7]UCLA Medical Scientist Training Program, David Geffen School of Medicine, University of California, Los Angeles, Los Angeles, CA, USA. [8]CFFT Lab, Cystic Fibrosis Foundation, Lexington, MA, USA. [9]Jonsson Comprehensive Cancer Center, University of California, Los Angeles, Los Angeles, CA, USA. [10]Eli and Edythe Broad Stem Cell Research Center, University of California, Los Angeles, Los Angeles, CA, USA. [11]Marsico Lung Institute/Cystic Fibrosis Center, University of North Carolina, Chapel Hill, NC, USA. [12]Division of Pulmonary Sciences and Critical Care Medicine, Department of Medicine and Department of Cell and Developmental Biology, University of Colorado Denver School of Medicine, Aurora, CO, USA. [13]Division of Pulmonary and Critical Care Medicine, David Geffen School of Medicine, University of California, Los Angeles, Los Angeles, CA, USA. [14]These authors contributed equally: Gianni Carraro, Justin Langerman. [15]These authors jointly supervised this work: Kathrin Plath, John E. Mahoney, Barry R. Stripp, Brigitte N. Gomperts. ✉e-mail: kplath@mednet.ucla.edu; jmahoney@cff.org; barry.stripp@cshs.org; bgomperts@mednet.ucla.edu

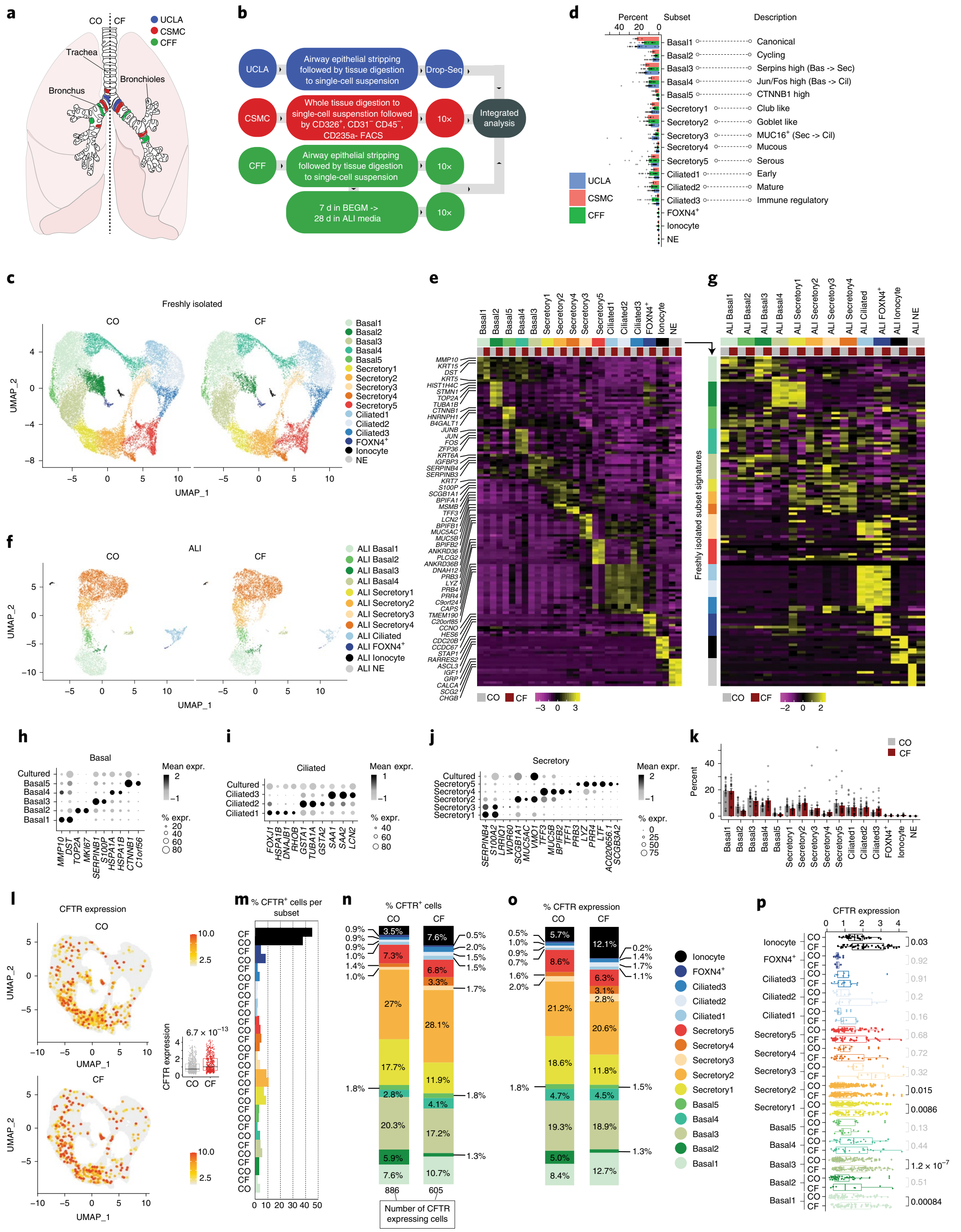

**Fig. 1 | Single-cell transcriptome atlas of the epithelium lining proximal airways of control donors and donors with end-stage CF lung disease. a**, Locations of cell procurement for scRNA-seq. **b**, Methodology used for cell isolation by each institution. **c**, Dimensional reduction of data generated from freshly isolated CO and CF airway epithelium, visualized by UMAP, with cells colored by subsets as shown in the key. **d**, Distribution of cell subsets by institution. Error bars show standard error of the mean. *n* for UCLA = 17 biologically independent samples, *n* for CSMS = 16 biologically independent samples and *n* for CFF = 5 biologically independent samples. **e**, Scaled expression of the top DEGs that inform specific cell subsets, for *k*-groups of CO and CF cells further separated by subset, visualized by heat map. **f**, Dimensional reduction of data generated from ALI cultures derived from samples shown above. Cells are colored by ALI-specific subsets, shown in the key at right. **g**, Heat map of the scaled expression of the same fresh tissue subset genes from **e** but shown for groups of ALI-control and CF cells split by subset. **h**–**j**, Comparison of subset-specific gene expression among fresh tissue subsets and cultured cells. **k**, Distribution of the average proportion of cell subsets per sample, comparing CO and CF cells. Error bars show standard error of the mean. *n* = 19 CF samples and 19 CO samples. **l**–**p**, *CFTR* expression in subset groups, key at right. **l**, *CFTR* expression across all subsets, shown on the UMAP and as a box plot of CO/CF versus expression level (**m**). Proportion of *CFTR*-expressing cells per each subset. **n**, Proportion of *CFTR*-expressing cells and (**o**) *CFTR* expression, for *CFTR*+ cells only, visualized by stacked column charts. **p**, Distribution of *CFTR* expression in all subsets, for *CFTR*+ cells only, divided by CO and CF status. *P* values (Wilcoxon test) shown at right indicate the significance of distribution differences between CO and CF per subset, bolded if $P < 0.05$. Whiskers show 1.5 times the interquartile range.

Secretory cells were divided into five specific subsets (Secretory1–5) that share defining gene signatures in CO and CF datasets (Fig. 1e). The Secretory1 subset includes cells characterized by expression of *SCGB1A1* (secretoglobin family member 1A1) and various serpin family members. Serpins regulate protein folding associated with maturation of secretory proteins[4] and define cells undergoing maturation into a secretory cell type with similarities to bronchiolar club cells[5]. The Secretory2 subset is composed of cells expressing mucins *MUC5B* and *MUC5AC*, *AGR2* (anterior gradient 2) and *SPDEF* (SAM-pointed domain-containing Ets-like factor), suggesting that they are goblet cells[6]. Cells in the Secretory3 subset can be distinguished by their expression of *DNAHs* (dynein axonemal heavy chain proteins), *ANKRDs* (ankyrin repeat domain proteins) and the mucins *MUC16* and *MUC4*, suggesting that they act as progenitors for ciliated cell differentiation. The Secretory4 subset is defined by expression of *MUC5B* and *TFF1* and *TFF3* (trefoil factor family domain peptides) and represents mucous-like cells that are distinct from goblet cells[7]. The Secretory5 subset contains a serous-like signature[7], expressing *LYZ* (lysozyme), *PRBs* and *PRRs* (proline-rich proteins) and *LTF* (lactoferrin) and represent glandular cell types of submucosal glands (SMGs) (Supplementary Table 2).

The three ciliated subsets (Ciliated1–3) (Fig. 1e) all share expression of markers and regulator of ciliogenesis, including *FOXJ1* (forkhead box protein J1)[8]. The Ciliated1 subset expressed markers of cilia pre-assembly[9], including *SPAG1* (sperm-associated antigen 1), *LRRC6* (leucin rich repeat containing 6) and *DNAAF1* (dynein axonemal assembly factor 1) most highly, whereas cells within the Ciliated2 subset showed the highest expression of markers of mature ciliated cells, including *TUBA1A* and *TUBB4B*. The Ciliated3 subset is characterized by *SAA1* and *SAA2* (serum amyloid A proteins), reflective of a pro-inflammatory state[10], suggesting that this subset of ciliated cells is either responding to or regulating immune responses.

Basal cells were divided into five subsets (Basal1–5) (Fig. 1d,e). The Basal1 subset is characterized by high expression of canonical basal cell markers, including *TP63* (tumor protein P63), *KRT5* and *KRT15* (cytokeratins 5 and 15) (Fig. 1e and Supplementary Table 2)[11]. Cells of the Basal2 subset showed enrichment for transcripts such as DNA *TOP2A* (topoisomerase II alpha) and *MKI67* (marker of proliferation Ki-67), suggesting that they represent proliferating basal cells (Fig. 1e and Supplementary Table 2). The Basal3 subset is enriched for the serpin family and might capture basal cells transitioning to a secretory phenotype[4] (Fig. 1e and Supplementary Table 2). The Basal4 subset is characterized by the highest expression of the AP-1 family members JUN and FOS, and the Basal5 subset uniquely expressed high levels of *CTNNB1* (β-catenin) (Fig. 1e and Supplementary Table 2).

We next sought to determine the extent to which these endogenous cellular subsets are recapitulated in the hBE cell differentiation air–liquid interface (ALI) culture system after 28 d of differentiation. We found that the previously identified cell types[2] observed in fresh isolates (basal, secretory, ciliated, *FOXN4*$^+$, ionocyte and NE) were also present in ALI cultures (Extended Data Fig. 1j) for both CO and CF-derived samples (Extended Data Fig. 1k). Based on gene expression differences, we were able to further define ALI-specific subsets of basal, secretory and ciliated cells (Fig. 1f). ALI Basal1, Basal2 and Basal4 showed overlapping marker gene expression with Basal1 (canonical), Basal3 (serpin-enriched) and Basal2 (proliferating) cells from freshly isolated tissue, respectively (compare Fig. 1e,g and Supplementary Tables 2 and 3). ALI Basal3 identified cells with high *KRT14* expression that lacked a counterpart basal cell subset in the fresh tissue data sets (Fig. 1e,g). ALI secretory and ciliated cell subsets lacked markers observed in the respective subsets of the freshly isolated tissue (Fig. 1e,g and Supplementary Table 3). Comparison of gene expression profiles between cells from ALI cultures and fresh tissue confirmed that significant differences were observed in subsets (Fig. 1h–j). Interestingly, we observed 46.8% fewer cells in the proliferative Basal2 subset and 26% fewer cells in the club-cell-like Secretory1 subset and a 44.6% increase in the proportion of cells in the inflammatory Ciliated3 subset in CF compared to CO samples (Fig. 1k). This implies that there are important differences when modeling CF in ALI cultures.

We next used our molecular atlas to examine *CFTR* gene expression. *CFTR* is expressed in many cells, with overall higher expression in CF compared to CO (Fig. 1l). Recent studies have proposed that ionocyte cells with high *CFTR* expression might represent tractable targets for restoration of *CFTR* expression in CF[2,3]. Although *CFTR* is overrepresented in ionocytes (Extended Data Fig. 1l), with more than 30% of all ionocytes expressing *CFTR* (Fig. 1m), they are rare cells. Most *CFTR*-expressing cells were secretory cells, followed by basal cells[12] (Fig. 1n). Secretory2 (goblet-like) cells and Basal3 (serpin-expressing) cells were the major cell subset contributors to *CFTR* expression (Fig. 1o). Comparison of *CFTR* expression between CO and CF samples showed cell-type-specific differences, with increases of expression in the CF ionocyte, Secretory1 (club-like), Secretory2 (goblet-like), Basal1 (canonical) and Basal3 (serpin-expressing) cell subsets (Fig. 1p). Our analysis confirms the specialized role of ionocytes for *CFTR* expression; however, it also establishes that secretory and basal cells account for the vast majority of *CFTR* expression in the proximal airway epithelium. Secretory and basal cells should, therefore, be included as candidates for therapeutic restoration of *CFTR* expression in CF.

## Secretory cells show increased anti-microbial activity in CF

We next validated the five identified subsets of secretory cells in the airway epithelium. Immunofluorescence (IF) staining of bronchi from CO samples confirmed the presence of SCGB1A1-immunoreactive cells that lacked staining of mucins MUC5B and MUC5AC, reflective of the Secretory1 subset (Fig. 2a,e). We detected cells expressing mucins MUC5B and MUC5AC (Fig. 2b,e), characteristic of goblet cells found in the Secretory2 subset[6]. In situ hybridization identified *MUC16*$^+$*FOXJ1*$^+$ cells indicative of the Secretory3 transitioning cell subset (Fig. 2c,e). IF analysis confirmed that the Secretory4 subset identifies a population present in both the surface airway epithelium and SMGs that expresses MUC5B but not SCGB1A1 or MUC5AC (Fig. 2b,e). IF also confirmed that the Secretory5 cell subset represents a glandular cell type of the SMGs, which produces lactoferrin but not MUC5AC or MUC5B (Fig. 2d,e).

To identify precise differences between CO and CF donors, we determined subset-specific gene expression changes that were validated across all three institutions, starting with the secretory subsets (Fig. 2f and Supplementary Table 2). In the Secretory1 (club-like) subset, CF samples showed downregulation of members of the *S100* gene family[13], which are important for tissue repair, differentiation and inflammation, suggesting possible repair defects in CF donors. In the Secretory2 (goblet-like) subset, immune response genes, such as *BPIFA1* and *BPIFB1* (ref. [14]), were upregulated in CF samples. The Secretory3 (*DNAH*-enriched) subset shows CF-specific increased expression of specific dyneins (*DNAH5*, *DNAH11*, *DNAH12* and *DNAAF1)*, which are linked to cilium assembly[15]. In the Secretory4 (mucous-like) subset, *ANG* (angiogenin) and *TFF1*, two molecules with a role in anti-microbial defense[16,17], were upregulated in CF compared to CO samples. The Secretory5 (serous-like) subset showed few CO–CF differences (Fig. 2f).

We further analyzed differences between CO and CF samples based on how co-regulated gene programs change. We applied an unbiased method that groups genes by transcript correlation. We found seven co-expression networks that were significantly altered between CO and CF in secretory cells, across all datasets (Fig. 2g, Extended Data Fig. 2a and Supplementary Table 4).

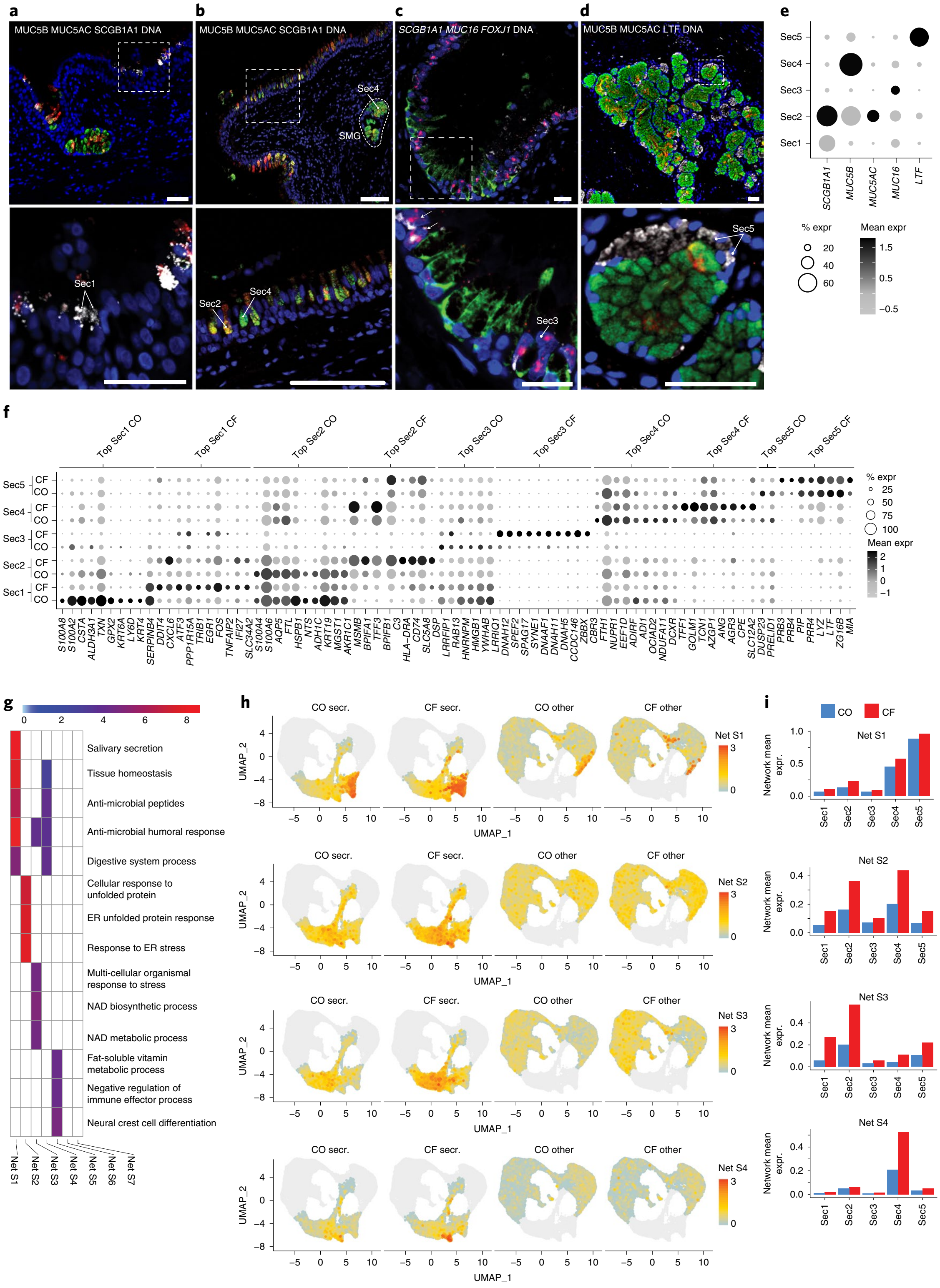

**Fig. 2 | Expansion of secretory function, including mucus secretion and anti-microbial activity, in CF secretory cells. a–e**, Validation of secretory cell subsets in sections from CO lung tissue. Lower panels are magnifications of the outlined dashed white boxes in the upper panels. **a**, **b**, Immunostaining for SCGB1A1 (white), mucins 5B (green), 5AC (red) and DNA (blue) identify secretory subsets 1, 2 and 4. **c**, In situ hybridization for *Scgb1a1* (green), *Muc16* (red) and *Foxj1* (white) identify secretory subset 3. **d**, Immunostaining for lactoferrin (LTF) (white), mucins 5B (green) and 5AC (red) identify secretory subset 5. **e**, Dot plot indicating the expression of level and frequency of genes from **a** to **d**. Scale bars: **a**,**d**, 50 µm; **b**, 100 µm; **c**, 20 µm. **f**, Dot plot indicating the expression level and frequency of DEGs from each secretory subset, across all subsets in CO and CF cells. Genes are expressed higher in either CO or CF, as indicated by the label at the top. **g**, For gene networks preferentially located in secretory cells, shown is a gene ontology heat map of the top three associated terms for each network with the term enrichment −log(*P* value) colored as displayed in the key. Networks with no associated ontology terms are blank (Net S6/S7). **h**, For each cell, the average mean expression of the genes in a given network is shown, visualized on a UMAP. Cells are split by Secretory or non-Secretory and CO or CF classification. **i**, Bar plots showing the average expression of all genes in individual secretory networks per secretory subset, in CO or CF cells.

Secretory networks 1–6 (Net S1–S6) are more highly expressed in CF versus CO secretory cells, whereas S7 is lower in secretory cells in CF samples (Fig. 2h and Extended Data Fig. 2b,c). Gene ontology analysis revealed that S1 and S4 have an anti-microbial signature[18]; the S2 program is related to endoplasmic reticulum (ER) stress[19]; and S3 is related to metabolic processes (Fig. 2g). The anti-microbial network S1 was most highly expressed in the Secretory4 and Secretory5 (serous-like) subsets, and expression of S4 was high specifically within the Secretory4 (mucous-like) subset (Fig. 2h,i), indicating that these subtypes in CF lungs have a specialized anti-microbial activity. Elevated ER stress from S2 was more pronounced among Secretory4 and Secretory2 (goblet-like) cells (Fig. 2h,i). S3 described a metabolic difference between Secretory2 (goblet-like) and Secretory1 (club-like) cells from CF versus CO samples (Fig. 2h,i), indicating that the surface hBE secretory cells might be more exhausted in CF samples. S5, marked by developmental ontology and expression of the Wnt signaling gene *FRZB*, and S6 and containing the Notch gene *HEY1*, was also elevated in CF samples (Supplementary Table 4). S7 was upregulated in CO versus CF samples and marked a small cell group expressing members of the *KLK* family, reported to be expressed in hBEs and implicated in regulation of airway inflammatory responses[20] (Extended Data Fig. 2). Secretory network transcription factors *LTF* (inflammatory) and *PRRX2* (developmental) were strongly upregulated in CF.

Overall, gene expression differences identified between CO and CF secretory cell subsets demonstrate overactive mucosal secretion, humoral immunity, anti-microbial activity and stress-related organelle maintenance, consistent with an increase in secretory function in the CF airway epithelium.

## An expanded ciliated cell gene expression program in CF

Next, we compared gene expression differences in ciliated cells between CO and CF samples. During ciliogenesis, a complex gene expression network is induced to generate the hundreds of structural and regulatory components of cilia[21,22]. Differential gene analysis revealed genes that were specific to ciliated cell subsets of either CO or CF samples and reproducible between datasets from all three institutions (Fig. 3a). The Ciliated1 subset showed higher expression of ciliogenesis transcripts, such as *DNAH5* (dynein axonemal heavy chain 5) and *SYNE1* and *SYNE2* (spectrin repeat containing nuclear envelope protein 1 and 2), in CF versus CO, suggesting an attempt to boost cilium biogenesis in CF lungs. Cells of the Ciliated2 subset showed higher expression of *AGR3* (anterior gradient 3) in CF samples, a gene that plays a role in ciliary beat frequency and motility[23]. CF cells of the Ciliated3 subset showed higher expression of *HLA-DPA1* and *HLA-DRB1* (major histocompatibility complex class II, DP alpha 1 and DR beta 1) genes that play an important role in the immune system.

Through Gene Expression Network Discovery (GEND), we also defined ten expression networks that are differentially expressed in ciliated cells (Fig. 3b and Extended Data Fig. 3a). Despite each network having distinct genes, many networks showed enrichment of ontology terms related to ciliogenesis and cilium movement (Net C1–C4 and C8; Fig. 3b, Extended Data Fig. 3b and Supplementary Table 4). Many transcriptional regulators were upregulated in CF networks, including *RFX3* and *FOXJ1*, which are proteins known to be involved in ciliogenesis[24]. Network C3 was associated with respiratory electron transport; C7 related to cellular repair and networks C3 and C5; and C6 contained genes with immune functions (Extended Data Fig. 3b). Smaller network C9 possessed inflammatory genes, and C10 had no ontology but also contained immune and ciliary genes (Extended Data Fig. 3b). Interestingly, the Ciliated3 subset showed an increase in expression of all of these networks in CF compared to CO (Fig. 3c,d and Extended Data Fig. 3b,c). We also found that the microtubule and ciliogenesis-related networks C1–C4 and C8 had higher expression among non-ciliated cells in CF compared to CO (Fig. 3c and Extended Data Fig. 3b,c).

Given this specific and unexpected upregulation of various cilium-related genes in non-ciliated cells of CF samples, we interrogated a manually curated list[25] of ten categories and 491 genes representing different phases of ciliogenesis (Fig. 3e, Extended Data Fig. 4 and Supplementary Table 5). We calculated the difference in proportion of cells that expressed a given ciliogenesis signature above a specific cutoff between CO and CF cell subsets. *FOXN4*$^+$ cells, previously reported to represent transitional *FOXJ1*$^+$ cells undergoing multi-ciliogenesis[2], were found to express ciliogenesis signature genes at a higher level in CF versus CO samples. Basal4, Basal5 and Secretory3 subsets also had higher expression of nearly all categories of ciliogenesis signature genes in CF versus CO samples, indicating enhanced secretory-to-ciliated cell transition in these cells (Fig. 3e).

The expansion of the ciliogenesis gene expression signature to basal cells suggested the possibility of direct basal-to-ciliated cell differentiation. To further investigate this, we examined CF and CO airway tissue for the presence of cells with dual expression of basal cell markers and transcripts associated with early ciliogenesis. In situ hybridization confirmed the presence of cells with dual expression of *KRT5* and *LRRC6*. These cells were located in the suprabasal position, a location consistent with their physical transition from a basal to a luminal location in the airway, and were significantly enriched in CF (Fig. 3f). Analysis at the protein level by IF for KRT5 and FOXJ1 confirmed the presence of this transitional population in CF (Fig. 3g). Taken together, these data suggest that CF airways display an overabundance of cells attempting to transition toward a ciliated cell fate compared to CO airways.

## Differences in metabolism and mitosis in CF versus CO basal cells

Basal cells are the primary stem cells of the proximal airways[26,27]. Seeking to confirm our molecular identification of basal cell subsets (Fig. 1c,d,e), we examined predicted cell surface markers CD266 (TNFRSF12A), from the Basal1 subset, and CD66 (CEACAM1/CEACAM5/CEACAM6) enriched in Basal3 (Extended Data Fig. 5a). Flow cytometry analysis on freshly isolated hBE cells confirmed the expected heterogeneity of these basal cell subsets. However, the same freshly cultured primary hBE cells appear to lose CD66-expressing subsets and uniformly express CD266 (Extended Data Fig. 5b), indicating that the Basal3 subset could not be maintained in vitro using culture conditions that were developed to expand basal cells.

Analysis of DEGs between basal cells of CO and CF samples revealed reproducible subset-specific differences (Fig. 4a). The CF Basal2 (proliferating) subset showed reduction of transcripts involved in cell division, whereas the CF Basal3 (serpin-expressing) subset showed lower expression of keratinization-associated genes[28,29], including *CSTA* (cystatin A) and *HSPB1* (heat shock protein B1). The CF Basal4 subset displayed increased expression of Fos and FosB proto-oncogenes (*FOS* and *FOSB*), whereas other AP-1 complex members (*JUN* and *JUNB*) were unchanged between CF and CO subsets.

Using the gene correlation grouping approach, we defined ten gene expression networks that were differentially regulated between CO and CF samples and were prominent in basal cells. Eight networks (Net B1–B4 and B7–B10) were more highly expressed in CO samples, and two networks (B5 and B6) were more highly expressed in CF samples (Fig. 4b, Extended Data Fig. 6 and Supplementary Table 4). The CF-enhanced B5 and B6 networks are related to surfactant metabolism and immune function (Fig. 4b and Extended Data Fig. 6a–c). Networks downregulated in CF versus CO samples were enriched for gene ontologies related to metabolism, cell division, epithelial cornification, immune functions and response to wounding (Fig. 4c and Extended Data Fig. 6a–c). Networks B1, B2 and B8 were more highly expressed in CO versus CF samples (Fig. 4c,d) and might signify patient-specific wound healing related to intubation. Several

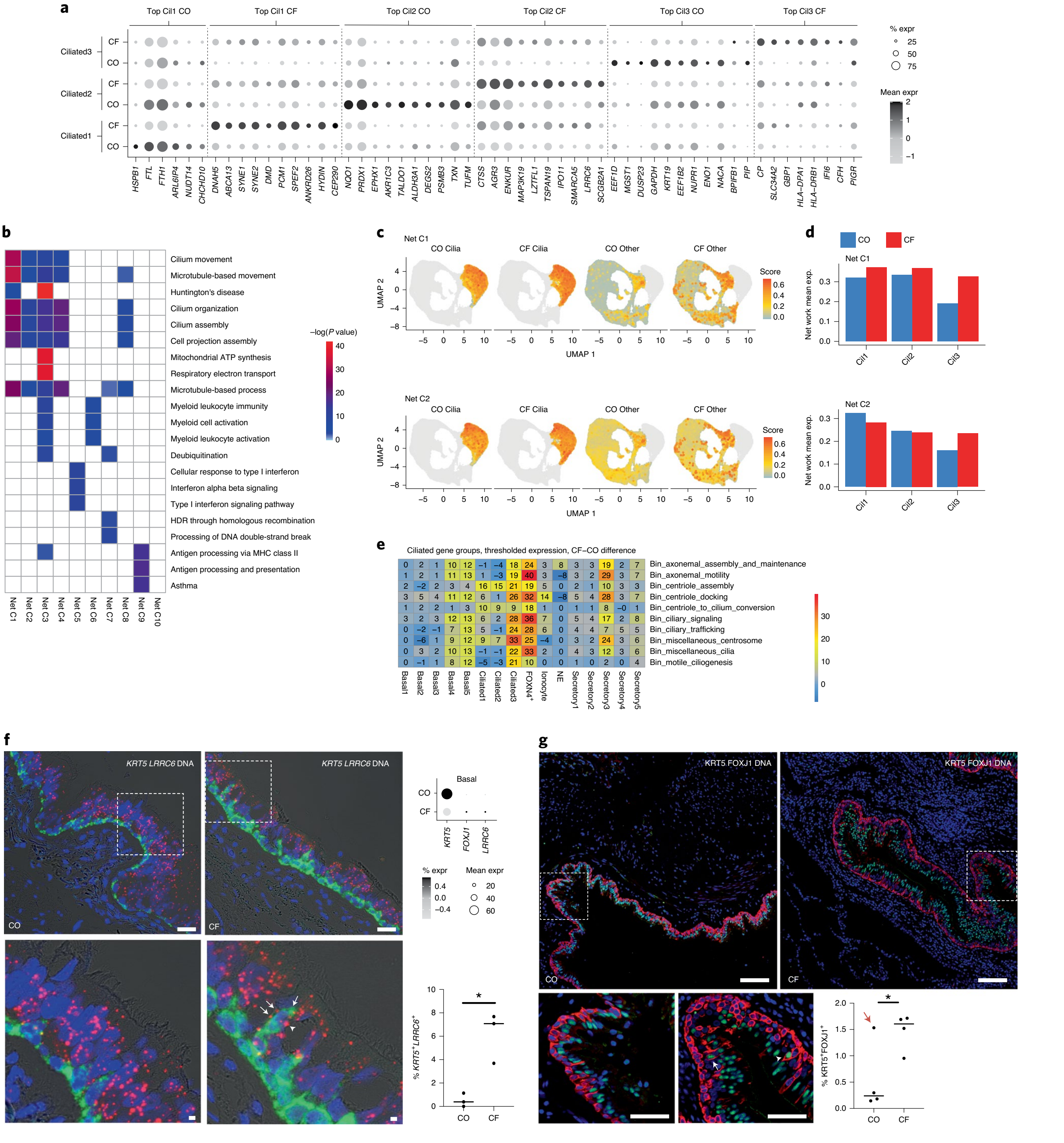

**Fig. 3 | Cilia-related gene expression is vastly expanded outside of the main cilia subgroups in CF. a**, Dot plot indicating the expression level and frequency of DEGs in each ciliated subset, for CO or CF cells. **b**, For gene networks preferentially expressed in ciliated cells, shown is a gene ontology heat map of the top three associated terms for each network with the term enrichment −log(*P* value) colored as displayed in the key. **c**, For each cell, the average mean expression of the genes in a given network is shown, visualized on a UMAP. Cells are split by Ciliated or non-Ciliated and CO or CF classification. **d**, Bar plots showing the average expression of all genes in individual ciliated networks per ciliated subset group, in CO or CF cells. **e**, For distinct categories of genes related to cilia biogenesis, the expansion of cilia gene expression is shown by a heat map indicating the proportional percent change in amount of cells in each subset expressing each category above a threshold, toward CF(+%) versus CO(−%) cells. The percent change number between CF and CO samples is given in each heat map cell and colored as indicated in the key at right. **f**, **g**, Validation of the basal-to-ciliated cell transition in sections from CO and CF lung tissue. Lower panels are magnifications of the outlined dashed white box in the upper panels. **f**, In situ hybridization for *Krt5* (green) and *Lrrc6* (red) with DNA (blue). Arrowhead indicates *Krt5*$^+$ basal cell in suprabasal position showing co-expression for *Lrrc6*. Scale bar low and high magnifications = 20 μm. Quantification of *Krt5*$^+$*Lrrc6*$^+$ basal cells in CO and CF airways is shown by the scatter plot. *$P$ = 0.0119 (Wilcoxon test). **g**, Immunostaining for KRT5 (red), FOXJ1 (green) and with DNA (blue). Arrowhead indicates KRT5$^+$ basal cell in suprabasal position showing co-expression for FOXJ1. Scale bar low magnification = 100 μm; high magnification = 50 μm. Quantification of KRT5$^+$FOXJ1$^+$ basal cells in CO and CF airway is shown by the scatter plot. *$P$ = 0.0486 (Wilcoxon test). The red arrow indicates a CO sample that showed levels of co-localization similar to CF. The bar shows the mean and $n$ = 3 (**f**) or 4 (**g**) for each sample.

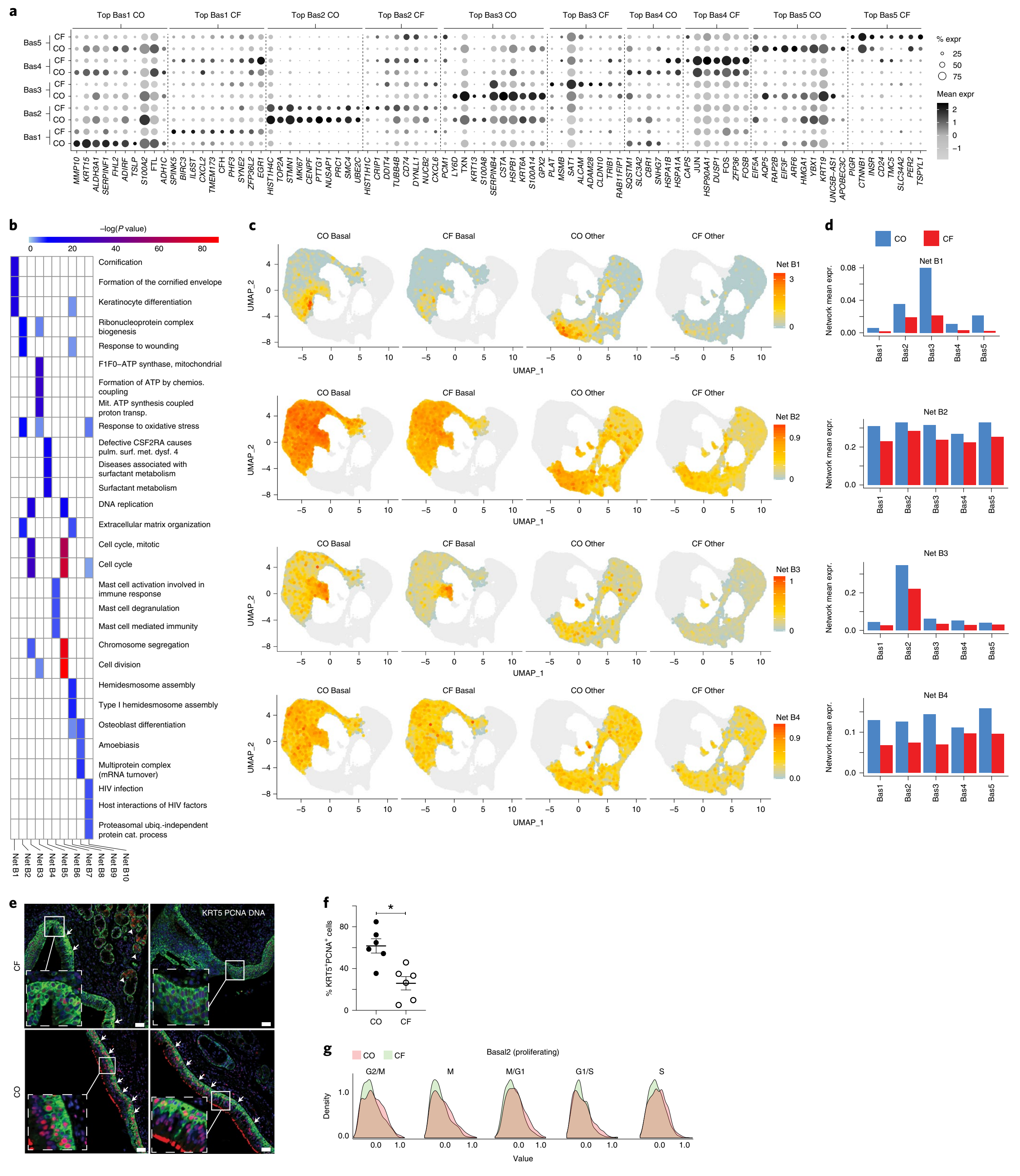

**Fig. 4 | Depletion of metabolic stability, basal epithelial function and cellular division is widespread in CF lung basal cells. a**, Dot plot indicating the expression level and frequency of DEGs in each basal subset, for CO or CF. **b**, For gene networks highly expressed in basal cells, shown is a gene ontology heat map of the top three associated terms for each network with the term enrichment –log(*P* value) colored as displayed in the key. **c**, For each cell, the average mean expression of the genes in a given network is shown, visualized on a UMAP. Cells are split by Basal or non-Basal and CO or CF classification. **d**, Bar plots showing the average expression of all genes in individual basal networks per basal subset group, in CO or CF cells. **e**, Immunostaining for KRT5 (green) and PCNA (red) in sections from CF and CO lung tissue. Nuclei are stained with DAPI (blue). Arrows indicate points of interest, whereas insets show magnification of the basal cell layer. Scale bar shows 50 µm. **f**, Quantification of $KRT5^+PCNA^+$ basal cells in CO and CF. $^*P = 0.0034$ (Wilcoxon test). Error bars show standard error of the mean and $n = 6$ for each sample. **g**, Expression distributions of cell cycle genes in CO and CF cells, in the proliferating Basal2 subset.

other molecular pathways were also downregulated in the basal cells of CF versus CO samples, including those related to response to oxidative stress and ATP synthesis (Net B2, B4 and B10; Fig. 4c,d). Strikingly, networks B3 and B7 revealed widespread downregulation of genes related to cell cycle in CF samples across all basal subsets but most strongly in the Basal2 (proliferating) subset (Fig. 4b,c,d).

To confirm the depletion of dividing basal cells in intact CF mucosa, we performed IF for co-localization of PCNA (marker of proliferation) and KRT5 (basal cell marker) in the same proximal airway samples used for transcriptomic analysis. We found that the PCNA-proliferative index of KRT5-immunoreactive cells in CF proximal airways was significantly reduced compared to similar airway regions of CO tissue (Fig. 4e,f). Furthermore, we confirmed a general reduction in all phases of the cell cycle among the proliferative Basal2 subset of CF samples compared to their CO counterparts (Fig. 4g). Next, using a subset of the same dissociated cells from CO and CF donors (analyzed in Fig. 1c), we established primary hBE cultures (passage 0–1)[30] and performed single-cell RNA sequencing (scRNA-seq). Interestingly, CO had a significantly higher Basal2 signature compared to CF (Extended Data Fig. 7), corroborating scRNA-seq and immunostaining data from freshly isolated cells. However, scRNA-seq data from these same hBE cultures after 28 d of differentiation at ALI showed a loss of this difference (Fig. 1f,g), showing that CF basal cells still have the potential to recover and replicate normally outside the CF lung microenvironment. Taken together, the reduction in proliferation of basal cells has important implications for airway repair and gene targeting of progenitor cells in CF.

## Discussion

We created an atlas of single-cell transcriptomes to reveal the diversity of epithelial cell subsets in normal airways, how the epithelium changes in airways of patients with end-stage CF lung disease and the relationship between epithelial cell phenotypes in intact airways versus ALI culture models. We confirmed the presence of cells transitioning from secretory to ciliated cells but also discovered transitional cell types that reflect direct differentiation of basal cells to the ciliated state. We verified that cells of this phenotype occupy the expected parabasal location within the pseudo-stratified epithelium of airways and showed that they are more abundant in CF compared to CO airway epithelium, reflecting an extension of the ciliated cell program in CF airways.

Our data provide key insights into the molecular pathology of epithelial cell defects seen in CF airways. Among these is a reduction in proliferating basal cells in CF, which might represent stem cell exhaustion resulting from prolonged epithelial turnover due to inflammation and injury in the CF airway. This finding did not confirm previous histological reports of increased basal cell proliferation in the CF airways[31,32]. Even though reductions in cycling basal cells in freshly isolated CF hBEs compared to CO were corroborated in vitro, it is not clear why CF airways also harbor increased transitional cell types relative to their CO counterparts.

Among the limitations of this study, we found inconsistencies in the representation of cellular subsets between the freshly isolated hBEs and the ALI culture model, which precluded determination of whether the observed increase in transitioning cells represents dysfunctional ciliogenesis or increased turnover of ciliated cells in the CF airway. We speculate that this is due, in part, to differences in synchronization of cellular turnover and the relative complexity of the airway microenvironment. Another limitation was the difficulty in inferring primary versus secondary effects of CFTR dysfunction from the scRNA-seq data, given that our study was limited to tissue from patients with CF who were undergoing transplantation for end-stage lung disease.

In summary, by leveraging the analysis of 38 patient samples across a three-institution consortium and assessing gene expression patterns that are common between datasets, we generated molecular atlases of control and CF proximal airway epithelium. Our data suggest that specific subsets of basal, secretory and ciliated cells have the potential to play a role in CF lung disease and provide a rich resource for the research community for discovery, drug development and validation. The molecular profiles of basal cell subsets described herein will guide strategies aimed at targeting gene corrective cargo to long-lived basal stem cells of the CF airway[33]. Furthermore, a molecular roadmap of the normal and CF airway provides a framework to assess therapeutic interventions aimed at correction of both electrolyte transport defects and broader changes in epithelial cell composition and function in airways of patients with CF.

## Online content

Any methods, additional references, Nature Research reporting summaries, source data, extended data, supplementary information, acknowledgements, peer review information; details of author contributions and competing interests; and statements of data and code availability are available at https://doi.org/10.1038/s41591-021-01332-7.

Received: 1 May 2020; Accepted: 24 March 2021;
Published online: 6 May 2021

## References

1. Carraro, G. et al. Single-cell reconstruction of human basal cell diversity in normal and idiopathic pulmonary fibrosis lungs. *Am. J. Respir. Crit. Care Med.* **202**, 1540–1550 (2020).
2. Plasschaert, L. W. et al. A single-cell atlas of the airway epithelium reveals the CFTR-rich pulmonary ionocyte. *Nature* **560**, 377–381 (2018).
3. Montoro, D. T. et al. A revised airway epithelial hierarchy includes CFTR-expressing ionocytes. *Nature* **560**, 319–324 (2018).
4. Pan, S., Iannotti, M. J. & Sifers, R. N. Analysis of serpin secretion, misfolding, and surveillance in the endoplasmic reticulum. *Methods Enzymol.* **499**, 1–16 (2011).
5. Rokicki, W., Rokicki, M., Wojtacha, J. & Dzeljijli, A. The role and importance of club cells (Clara cells) in the pathogenesis of some respiratory diseases. *Kardiochir. Torakochirurgia Pol.* **13**, 26–30 (2016).
6. Chen, G. et al. SPDEF is required for mouse pulmonary goblet cell differentiation and regulates a network of genes associated with mucus production. *J. Clin. Invest.* **119**, 2914–2924 (2009).
7. Widdicombe, J. H. & Wine, J. J. Airway gland structure and function. *Physiol. Rev.* **95**, 1241–1319 (2015).
8. Yu, X., Ng, C. P., Habacher, H. & Roy, S. Foxj1 transcription factors are master regulators of the motile ciliogenic program. *Nat. Genet.* **40**, 1445–1453 (2008).
9. Horani, A. et al. Establishment of the early cilia preassembly protein complex during motile ciliogenesis. *Proc. Natl Acad. Sci. USA* **115**, E1221–E1228 (2018).
10. Ather, J. L. et al. Serum amyloid A activates the NLRP3 inflammasome and promotes Th17 allergic asthma in mice. *J. Immunol.* **187**, 64–73 (2011).
11. Rock, J. R., Randell, S. H. & Hogan, B. L. Airway basal stem cells: a perspective on their roles in epithelial homeostasis and remodeling. *Dis. Model Mech.* **3**, 545–556 (2010).
12. Okuda, K. et al. Secretory cells dominate airway CFTR expression and function in human airway superficial epithelia. *Am. J. Respir. Crit. Care Med.* https://doi.org/10.1164/rccm.202008-3198OC (2020).
13. Xia, C., Braunstein, Z., Toomey, A. C., Zhong, J. & Rao, X. S100 proteins as an important regulator of macrophage inflammation. *Front. Immunol.* **8**, 1908 (2017).
14. Akram, K. M. et al. An innate defense peptide BPIFA1/SPLUNC1 restricts influenza A virus infection. *Mucosal Immunol.* **11**, 1008 (2018).
15. Thomas, J. et al. Transcriptional control of genes involved in ciliogenesis: a first step in making cilia. *Biol. Cell* **102**, 499–513 (2010).
16. Mihalj, M. et al. Differential expression of *TFF1* and *TFF3* in patients suffering from chronic rhinosinusitis with nasal polyposis. *Int. J. Mol. Sci.* **20**, 5461 (2019).
17. Eckmann, L. Defence molecules in intestinal innate immunity against bacterial infections. *Curr. Opin. Gastroenterol.* **21**, 147–151 (2005).
18. Bals, R., Weiner, D. J. & Wilson, J. M. The innate immune system in cystic fibrosis lung disease. *J. Clin. Invest.* **103**, 303–307 (1999).

19. Tang, A. C. et al. Endoplasmic reticulum stress and chemokine production in cystic fibrosis airway cells: regulation by STAT3 modulation. *J. Infect. Dis.* **215**, 293–302 (2017).
20. Petraki, C. D., Papanastasiou, P. A., Karavana, V. N. & Diamandis, E. P. Cellular distribution of human tissue kallikreins: immunohistochemical localization. *Biol. Chem.* **387**, 653–663 (2006).
21. Brooks, E. R. & Wallingford, J. B. Multiciliated cells. *Curr. Biol.* **24**, R973–982 (2014).
22. Hoh, R. A., Stowe, T. R., Turk, E. & Stearns, T. Transcriptional program of ciliated epithelial cells reveals new cilium and centrosome components and links to human disease. *PLoS ONE* **7**, e52166 (2012).
23. Bonser, L. R. et al. The endoplasmic reticulum resident protein AGR3. required for regulation of ciliary beat frequency in the airway. *Am. J. Respir. Cell Mol. Biol.* **53**, 536–543 (2015).
24. Didon, L. et al. RFX3 modulation of FOXJ1 regulation of cilia genes in the human airway epithelium. *Respir. Res* **14**, 70 (2013).
25. Goldfarbmuren, K. C. et al. Dissecting the cellular specificity of smoking effects and reconstructing lineages in the human airway epithelium. *Nat. Commun.* **11**, 2485 (2020).
26. Wells, J. M. & Watt, F. M. Diverse mechanisms for endogenous regeneration and repair in mammalian organs. *Nature* **557**, 322–328 (2018).
27. Teixeira, V. H. et al. Stochastic homeostasis in human airway epithelium is achieved by neutral competition of basal cell progenitors. *eLife* **2**, e00966 (2013).
28. Tezuka, T., Takahashi, M. & Katsunuma, N. Cystatin alpha is one of the component proteins of keratohyalin granules. *J. Dermatol* **19**, 756–760 (1992).
29. O'Shaughnessy, R. F. et al. AKT-dependent HspB1 (Hsp27) activity in epidermal differentiation. *J. Biol. Chem.* **282**, 17297–17305 (2007).
30. Randell, S. H., Walstad, L., Schwab, U. E., Grubb, B. R. & Yankaskas, J. R. Isolation and culture of airway epithelial cells from chronically infected human lungs. *Vitr. Cell Dev. Biol. Anim.* **37**, 480–489 (2001).
31. Voynow, J. A., Fischer, B. M., Roberts, B. C. & Proia, A. D. Basal-like cells constitute the proliferating cell population in cystic fibrosis airways. *Am. J. Respir. Crit. Care Med.* **172**, 1013–1018 (2005).
32. Leigh, M. W., Kylander, J. E., Yankaskas, J. R. & Boucher, R. C. Cell proliferation in bronchial epithelium and submucosal glands of cystic fibrosis patients. *Am. J. Respir. Cell Mol. Biol.* **12**, 605–612 (1995).
33. King, N. E. et al. Correction of airway stem cells: genome editing approaches for the treatment of cystic fibrosis. *Hum. Gene Ther.* **31**, 956–972 (2020).

**Publisher's note** Springer Nature remains neutral with regard to jurisdictional claims in published maps and institutional affiliations.

## Methods

**Study population.** Human lung tissue was obtained from Cedars-Sinai Medical Center (CSMC), the University of North Carolina at Chapel Hill (UNC) CF Center Tissue Procurement and Cell Culture Core, the University of Texas Southwestern (UTSW), the University of California, Los Angeles (UCLA), the University of Southern California (USC) and the University of Iowa. CF tissue was obtained from donors with end-stage disease undergoing transplantation, whereas human lungs unsuitable for transplantation were obtained from Carolina Donor Services, the National Disease Research Interchange or the International Institute for Advancement of Medicine. Human lung tissues were procured under each institution's approved institutional review board protocols: no. 00035396 (CSMC), no. 03-1396 (UNC), no. 1172286 (CFF and WCG-Copernicus Group WIRB) and no. 16-000742 (UCLA). Informed consent was obtained from lung donors or their authorized representatives.

All requests for raw and analyzed data and materials will be promptly reviewed by B.G. to verify whether the request is subject to any intellectual property considerations.

**IF staining and in situ hybridization.** Proximal airway from control donors and CF explant tissues were fixed in formalin for 24 h, embedded in paraffin and sectioned at 10-µm thickness. Sections were deparaffinized at 60 °C followed by washes in xylene (VWR, 89370-088) and rehydrated through a gradient of decreasing ethanol concentration (Thermo Fisher Scientific, BP28184). Heat-induced epitope retrieval was performed using a steamer (Hamilton-Beach, 37530) in antigen retrieval solution (Vector Laboratories, H-3301). Slides were blocked with 5% normal donkey serum and normal goat serum in IF buffer (1× PBS/1% BSA/0.3% Triton X-100) for 1 h at room temperature and incubated with primary antibodies PCNA (Cell Signaling, 13110), KRT5 (BioLegend, 905901), SCGB1A1 (R&D, MAB4218), FOXJ1, MUC5AC, LTF (Thermo Fisher Scientific, 14-9965-82, MA5-12175 and PA5-19036) and MUC5B (Sigma-Aldrich, HPA008246) overnight at 4 °C. After washes in 1× TBS, sections were incubated with secondary antibody for 1 h at room temperature. In situ hybridization was performed using RNAscope Multiplex Fluorescent Assay v2 (Advanced Cell Diagnostics) with probes (Hs-KRT5-O1, Hs-SCGB1A1, Hs-MUC16-C2, Hs-FOXJ1-C3 and Hs-LRRC6-C2), following manufacturer instructions. Nuclei were stained by incubation in DAPI (Thermo Fisher Scientific, D1306). Sections were mounted in Fluomount-G (SouthernBiotech 0100-01). Sections were imaged at ×20 or ×40 magnification using a Leica DMi8 or a Zeiss LSM 780. Tile scans were created using Leica's LAS X software (Leica Microsystems) or Zen Blue software (Zeiss). For IF, images were cleaned using Photoshop (Adobe) by creating a masking layer to select for expressing cells, and, from this mask, overlapping co-expressing cells were isolated (Extended Data Fig. 8). These images were then converted to 8-bit and analyzed on Fiji (Image J with plugins)[34] by setting appropriate thresholds, creating a binary mask and performing a watershed segmentation (Extended Data Fig. 8). Segmented images were then measured, and counts were obtained using a minimum area of 100 pixels and a maximum area of two standard deviations above the mean area of pixels (Extended Data Fig. 8). The basal cell proliferative index was obtained by dividing the number of isolated PCNA-immunoreactive nuclei by the total number of KRT5-immunoreactive cells. Representative tile scan images are shown in Extended Data Fig. 8 for CO and CF samples, respectively. For in situ hybridization experiments, images were processed in a similar way using Fiji. All data were compared using an unpaired Student's *t*-test; results were considered significant when $P \leq 0.05$.

**Cell isolation.** Tissue at the CSMC site was processed to generate single-cell suspensions of isolated epithelial cells as described previously[35], with the following modifications. Tissue was enzymatically digested with Liberase followed by gentle scraping of epithelial cells off the basement membrane. Remaining tissue was then finely minced and washed with rocking in Ham's F-12 (Corning) at 4 °C for 5 min, followed by centrifugation at 4 °C for 5 min at 600*g*. Minced cleaned tissue was then incubated in DMEM/F-12 (Thermo Fisher Scientific) containing 1× Liberase (Sigma-Aldrich), incubated at 37 °C with rocking for 45 min. Dissociated cells recovered by scraping or by tissue mincing were then combined, and epithelial cells were enriched in a two-step process involving magnetic bead (MicroBeads, Miltenyi Biotec) depletion of erythrocytes, leukocytes and endothelial cells using antibodies to CD235a (MACS, CD235a 130-050-501), CD45 (MACS, CD45 130-045-801, Miltenyi Biotec) and CD31 (MACS, CD31 130-091-935, Miltenyi Biotec). Fluorescence-activated cell sorting (FACS) was used to enrich epithelial cells based on negative surface staining for CD235a (HI264, 349106), CD45 (2D1,368522) and CD31 (WM59, 303124) (BioLegend) and positive staining for CD326 (CO17-1A, 369820) (BioLegend). Stained cells were washed in HBSS containing 2% FBS, resuspended and placed on ice for FACS using a BD Influx cell sorter and the BD FACS Sortware software (Becton Dickinson) (Extended Data Fig. 9). Viability was determined by staining cell preparations with 7AAD (BioLegend), propidium iodide (BioLegend) or DAPI (Thermo Fisher Scientific), 15 min before cell sorting.

Tissue at the CFF site was processed as previously described[30,36]. Briefly, large airways (8 mm in diameter and larger) were rinsed with PBS, and soft tissue and lung parenchyma were dissected away, exposing intrapulmonary airways. Isolated airways were cut into ~2–3-cm segments and along their longitudinal axis to expose the airway lumen. After dissection, tissue was collected and washed in ice-cold PBS supplemented with 65 mg of diothreitol and 1.25 mg of deoxyribonuclease I (DNase). Tissue was then washed with cold basal BronchiaLife Airway media (Lifeline Cell Technology, cat. no. LL-0023) before digestion for 6–24 h in 0.25% Protease XIV (Sigma-Aldrich) supplemented with ACT-V (amphotericin B (Sigma-Aldrich, cat. no. A2942), antibiotic-antimycotic (Gibco, cat. no. 15240-062), ceftazidime HCL (Sigma-Aldrich, cat. no. C3809), tobramycin (Sigma-Aldrich, cat. no. T4014) and vancomycin (Sigma-Aldrich, cat. no. V8138)). After digestion, the luminal side of bronchial tissue was scraped using a convex scalpel and rinsed to remove airway epithelial cells. Isolated airway epithelial cells were then either 1) treated with Accumax (Sigma-Aldrich, cat. no. A7089) to yield a single-cell suspension and processed for single-cell transcriptional analysis or 2) plated and grown on collagen-coated flasks in BronchiaLife nedia + ACT-V until clearance of bacterial/fungal infections. Standard culture techniques were followed, using complete BronchiaLife media.

Tissue at the UCLA site was processed as previously described[37–41]. Tissue from the bronchi and carina were dissected, cleaned and incubated in 16 U ml$^{-1}$ of Dispase for 1 h at room temperature. Tissues were then incubated in 0.5 mg ml$^{-1}$ of DNase for another hour at room temperature. The airway epithelium was then stripped and incubated in Accumax (Sigma-Aldrich, cat. no. A7089) for 1 h with shaking at 37 °C; cells were filtered and centrifuged at 800*g* for 5 min; and the cell pellet was resuspended in media to a single-cell suspension before being used immediately for Drop-Seq. For SMG microdissection, the remaining tissue after airway epithelial stripping was left in Liberase at 4 °C overnight (diluted fresh 1:40 with PBS from 2.5 mg ml$^{-1}$ of stock), and SMGs were recovered by microdissection. Isolated SMGs were digested in trypsin for 30 min to yield a single-cell suspension. An equal volume of media was added to neutralize the trypsin and filtered through a 40-µm filter to generate a suspension of single cells. Cells were centrifuged at 800*g* for 5 min, and then the cell pellet was suspended in media and immediately processed for Drop-Seq.

**Generation of ALI cultures.** hBE cells were isolated and cultured as previously described[30,36]. Briefly, after initial airway expansion in BronchiaLife on BioCoat collagen-coated T-75 flasks (Corning, cat. no. 356487), cells were lifted by Versene (Gibco, cat. no. 15040-066) followed by Accutase (Sigma-Aldrich, cat. no. SCR005) incubations and either 1) prepared for scRNA-seq using the 10× Genomics platform (described below) and referred to primary hBE (passage 0–1) or 2) plated to transwell filter membranes (Corning, cat. no. 3470) and differentiated for 28 d, referred to as ALI cultures. hBE seeding density of transwell filters was $5.0 \times 10^5$ per cm$^2$ in BronchiaLife media for 24 h, followed by media change to the ALI medium formulation described by Neuberger et al.[36]. Cultures remained submerged for the first 96 h, before removal of apical medium, which initiated the ALI time course. hBE ALI cultures were maintained for 28 d, with 48-h media changes. On day 28, hBE ALI samples were collected by a thorough PBS wash followed by incubation in AccuMax (Sigma-Aldrich, cat. no. A7089) for 1–2 h followed by microscopic evaluation until a single-cell suspension was identified. After a wash with cold PBS, cells were passed through a 40-µm filter and counted before single-cell capture and RNA sequencing. To evaluate basal cell subsets, freshly isolated or ALI day 0 cells were stained with PE-Cy7 anti-human CD31 and CD45 (BioLegend, 303117 and 368531), AF488 anti-human CD326 (BioLegend, 324209), PerCP-Cy5.5 anti-human CD271 (BioLegend, 345111), AF647 anti-human CD66 (BioLegend, 342307) and PE anti-human CD266 (BioLegend, 314004). Viability was determined by staining cell preparations with DAPI. FACS was performed using a BD Influx cell sorter for freshly isolated cells and a Sony SH800S for ALI cells. IF staining was performed using TP63 (Cell Signaling Technology, D2K8X), KRT5 (BioLegend, Poly9059), BPIFA1 (R&D, AF1897) or TUBA4A (Sigma-Aldrich, T7471).

**Single-cell library generation and sequencing.** Single cells at the CSMC and CFF sites were captured using a 10× Chromium device (10× Genomics), and libraries were prepared according to the Single-Cell 3′ v2 or v3 Reagent Kits user guide (10× Genomics, https://www.10xgenomics.com/products/single-cell/). Cellular suspensions were loaded on a Chromium Controller instrument (10× Genomics) to generate single-cell Gel Bead-In-EMulsions (GEMs). Reverse transcription (RT) was performed in a Veriti 96-well thermal cycler (Thermo Fisher Scientific). After RT, GEMs were harvested, and the complementary DNA underwent size selection with SPRIselect Reagent Kit (Beckman Coulter). Indexed sequencing libraries were constructed using the Chromium Single-Cell 3′ Library Kit (10× Genomics) for enzymatic fragmentation, end-repair, A-tailing, adapter ligation, ligation cleanup, sample index polymerase chain reaction (PCR) and PCR cleanup. Library quality control was performed by the Agilent Technologies Bioanalyzer 2100 using the High Sensitivity DNA Kit (Agilent Technologies, cat. no. 5067-4626) and quantitated using the Universal Library Quantification Kit (Kapa Biosystems, cat. no. KK4824. Sequencing libraries were loaded on a NextSeq 500 (Illumina) for the CFF site and a NovaSeq 6000 (Illumina) for the CSMC site.

At UCLA, cells were resuspended in 0.01% BSA in 1× PBS at approximately 150 cells per µl. Cells were co-flowed with barcoded beads (ChemGenes) in a FlowJEM microfluidics device (PDMS Drop-Seq) and isolated for RT as described according to the Drop-Seq protocol[42]. Libraries were constructed with KAPA polymerase and Nextera XT preparation kit as previously described and paired-end sequenced on a HiSeq 4000 (Illumina).

**Data analysis.** For the CSMC and CFF sites, Cell Ranger software (10× Genomics) was used for mapping and barcode filtering. Briefly, the raw reads were aligned to the transcriptome using STAR[43], using a hg38 transcriptome reference from GENCODE 25 annotation. Expression counts for each gene in all samples were collapsed and normalized to unique molecular identifier (UMI) counts, yielding a large digital expression matrix with cell barcodes as rows and gene identities as columns.

At UCLA, raw sequencing data were filtered by read quality and adapter- and polyA-trimmed, and reads satisfying a length threshold of 30 nucleotides were aligned to the human genome using Bowtie2. Aligned reads were tagged to gene exons using Bedtools Intersect (v2.26.0). DGE matrices were then generated by counting gene transcripts for all cells within each sample using custom Python scripts (Drop-Seq Runner, https://github.com/ShanSabri/dropseq_runner). Cell barcodes were merged within 1 Hamming distance.

Data analysis was performed with Seurat 3.0 (ref. [44]) with some variation that will be described.

For all data, quality control and filtering were performed to remove cells with low number of expressed genes (threshold $n \geq 200$) and elevated expression of apoptotic transcripts (threshold mitochondrial genes <15%). Only genes detected in at least three cells were included. Each dataset was run with SoupX analysis package to remove contaminant 'ambient' RNA derived from lysed cells during isolation and capture[45]. Correction was performed on the basis of genes with a strong bimodal distribution and for which the 'ambient' RNA expression was overlapping with a gene signature of a known cell type. The 'adjustCounts' function of SoupX was used to generate corrected count matrices. To minimize doublet contamination for each dataset, quantile thresholding was performed to identify high UMI using a fit model generated using the multiplet's rate to recovered cells proportion, as indicated by 10× Genomics (https://kb.10xgenomics.com/hc/en-us/articles/360001378811-What-is-the-maximum-number-of-cells-that-can-be-profiled-). The raw expression matrix was processed with SCTransform wrapper in Seurat. Mitochondrial and ribosomal mapping percentages were regressed to remove them as a source of variation. Each dataset was first processed separately with principal component analysis (PCA) using the 5,000 most variable genes as input, followed by clustering with the Leiden algorithm[46] using the first 30 independent components and a resolution of 0.5 for clustering. Two-dimensional visualization was obtained with UMAP[47]. Identified AT2 (SFTP$^+$), immune (CD45$^+$) and endothelial (PECAM1$^+$) contaminating clusters were removed by subsetting the Seurat object, using the 'subset' function, before proceeding to data integration. After removal of contaminating cells, the raw expression matrix was processed with SCTransform. log1p logarithmically transformed data were obtained for each dataset and scaled as Pearson residuals. Pearson residual data were then used to integrate datasets following the Seurat workflow, using the PrepSCTIntegration function. Integrated datasets were used for downstream analysis. Datasets were processed with PCA using the 5,000 most variable genes as input, followed by clustering with the Leiden algorithm using the first 30 independent components and a resolution of 3 for fine clustering. Two-dimensional visualization was obtained with UMAP. To identify DEGs between clusters, model-based analysis of single-cell transcriptomics (MAST)[48] was used within Seurat's FindMarkers function. For this analysis, the *P*-value adjustment was performed using Bonferroni correction based on the total number of genes. To identify major cell types in our normal integrated datasets, previously published lung epithelial cell-type-specific gene lists[2] were used to create cell-type-specific gene signatures using a strategy previously described[49]. All analyzed features were binned based on averaged expression, and the control features were randomly selected from each bin. Clusters identified with the Leiden algorithm were assigned to major cell types on the basis of rounds of scoring and refinement. Each refinement was produced using transcripts differentially expressed within the best identified clusters from the previous scoring. Within each major cell type, Leiden clustering and differential gene expression were used to infer subclustering. Gene lists used as cell-type-specific and cluster-specific signatures are shown in supplementary tables (Supplementary Table 2). Violin plots show expression distribution and contain a box plot showing median, interquartile range and lower and upper adjacent values.

**Definition of genes with global expression differences in CF samples.** To define genes with altered gene expression states in the CF lungs, the expression of all detected genes was averaged across all cells (including all cells from CF and CO samples) for the datasets of each of the three institutions (UCLA, CSMI and CFF). For each institutional gene set, a ratio was then calculated between the CF and CO expression values for all cells. This ratio was then used to classify genes as upregulated or downregulated in CF, using the following criteria:

(i) Genes with a CF/CO ratio > 1.25, found in the data of all three institutions, were called CF.UP.Strong.
(ii) Genes with a CF/CO ratio between 1.25 and 1.1, in the data of all institutions, were called CF.UP.Weak.
(iii) Genes with a CF/CO ratio < 0.75, found in the data of all three institutions, were called CF.DOWN.Strong.
(iv) Genes with a CF/CO ratio between 0.75 and 0.9, found in all institutions, were called CF.DOWN.Weak.
(v) Importantly, these criteria required that the respective expression changes were found in each of the institutional datasets.

**GEND.** To define gene expression networks, we followed the following steps. First, cells were separated into groups based on their classification as Basal, Ciliated or Secretory cell types, as defined in Fig. 1c. Second, for each group of cells, a Pearson correlation coefficient matrix was calculated for all gene-versus-gene normalized transcript counts. For our data, the optimal cutoff for gene–gene correlation was evaluated and found to be $r > 0.20$, based on prior optimization. This step created the largest networks while limiting the formation of small networks. Gene–gene correlations with $r < 0.2$ were discarded. Third, from this filtered gene expression correlation matrix, we took only the pairwise interactions that represent each gene's top correlate. These were merged by connecting all mentions of a genes into a web index. Fourth, webs were tested for average expression correlation to other webs by computing the average expression of all genes in each network for 50 cell clusters (derived by *k*-means clustering of the UMAP coordinates) and then calculating a Pearson correlation coefficient matrix for these web–web k-mer expression relationships. Finally, all webs above 0.8 correlation were merged in a similar manner to the gene correlates, forming networks. Networks with fewer than five genes were discarded.

The GEND method initially determined gene correlations within each major cell type of the lung tissue. At this point, genes in a specific major cell type network could also be found in networks from the other two major cell types (an example of this is documented in the manuscript by the expression of cilia genes outside the ciliated cell subtype in Fig. 3). To avoid describing duplicate gene expression patterns for given genes, we assigned shared genes solely to the largest network (for example, overlapping genes from a small network containing cilia-related genes, defined in basal cells, were assigned to a larger network found in ciliated cells). Nearly all small networks that had genes removed by assignation to a different network during this step were later removed by the filtration criteria below.

To determine which networks were altered in CF cells compared to CO cells, we calculated the average expression level of all genes in each network, per major cell type. We took networks with the strongest cell-type-specific CF-versus-CO ratios (>10% for the major cell type assayed) and tested the cell subtype expression for significance using Bonferroni-corrected two-tailed *t*-tests. Networks were then filtered for a change in at least one subtype-specific CF/CO ratio of at least 20% and an adjusted *P* value less than 0.05. Networks that failed these criteria or that were depleted of over 50% of genes during the shared gene assignation stage were given an X designator (for example, Net XS17) and not used further in the analysis, although they are provided in Supplementary Table 4.

Expression threshold differences of networks were determined by applying a cutoff to all cells' average expression of a network, set at 30% of the third-maximum cell's expression level, for CO and CF cells separately to determine the percentile of each cell in each subset cluster, and then subtracting them to report the difference in those percentiles. Gene ontology enrichments were determined using the Metascape tool[50].

**Reporting Summary.** Further information on research design is available in the Nature Research Reporting Summary linked to this article.

## Data availability

Sequence data that support the findings of this study have been deposited in the National Center for Biotechnology Information Gene Expression Omnibus 'GenBank' with accession code GSE150674.

## References

34. Schindelin, J. et al. Fiji: an open-source platform for biological-image analysis. *Nat. Methods* **9**, 676–682 (2012).
35. Xu, Y. et al. Single-cell RNA sequencing identifies diverse roles of epithelial cells in idiopathic pulmonary fibrosis. *JCI Insight* **1**, e90558 (2016).
36. Neuberger, T., Burton, B., Clark, H. & Van Goor, F. Use of primary cultures of human bronchial epithelial cells isolated from cystic fibrosis patients for the pre-clinical testing of CFTR modulators. *Methods Mol. Biol.* **741**, 39–54 (2011).
37. Aros, C. J. et al. High-throughput drug screening identifies a potent Wnt inhibitor that promotes airway basal stem cell homeostasis. *Cell Rep.* **30**, 2055–2064 (2020).
38. Hegab, A. E. et al. Isolation and in vitro characterization of basal and submucosal gland duct stem/progenitor cells from human proximal airways. *Stem Cells Transl. Med.* **1**, 719–724 (2012).
39. Hegab, A. E. et al. Aldehyde dehydrogenase activity enriches for proximal airway basal stem cells and promotes their proliferation. *Stem Cells Dev.* **23**, 664–675 (2014).

40. Hegab, A. E., Ha, V. L., Attiga, Y. S., Nickerson, D. W. & Gomperts, B. N. Isolation of basal cells and submucosal gland duct cells from mouse trachea. *J. Vis. Exp.* **14**, e3731 (2012).
41. Paul, M. K. et al. Dynamic changes in intracellular ROS levels regulate airway basal stem cell homeostasis through Nrf2-dependent Notch signaling. *Cell Stem Cell* **15**, 199–214 (2014).
42. Macosko, E. Z. et al. Highly parallel genome-wide expression profiling of individual cells using nanoliter droplets. *Cell* **161**, 1202–1214 (2015).
43. Dobin, A. et al. STAR: ultrafast universal RNA-seq aligner. *Bioinformatics* **29**, 15–21 (2013).
44. Butler, A., Hoffman, P., Smibert, P., Papalexi, E. & Satija, R. Integrating single-cell transcriptomic data across different conditions, technologies, and species. *Nat. Biotechnol.* **36**, 411–420 (2018).
45. Young, M. D. & Behjati, S. SoupX removes ambient RNA contamination from droplet-based single-cell RNA sequencing data. *GigaScience* **9**, giaa151 (2020).
46. Traag, V. A., Waltman, L. & van Eck, N. J. From Louvain to Leiden: guaranteeing well-connected communities. *Sci. Rep.* **9**, 5233 (2019).
47. Becht, E. et al. Dimensionality reduction for visualizing single-cell data using UMAP. *Nat. Biotechnol.* https://doi.org/10.1038/nbt.4314 (2018).
48. Finak, G. et al. MAST: a flexible statistical framework for assessing transcriptional changes and characterizing heterogeneity in single-cell RNA sequencing data. *Genome Biol.* **16**, 278 (2015).
49. Tirosh, I. et al. Single-cell RNA-seq supports a developmental hierarchy in human oligodendroglioma. *Nature* **539**, 309–313 (2016).
50. Zhou, Y. et al. Metascape provides a biologist-oriented resource for the analysis of systems-level datasets. *Nat. Commun.* **10**, 1523 (2019).

## Acknowledgements

We would like to thank S. Reynolds for helpful input in reviewing this manuscript. This work was supported by the Cystic Fibrosis Foundation (GOMPER17XX0 (B.N.G.), STRIPP17XX0 (B.R.S.), CARRAR19G0 (G.C.) and BOUCHE15R0 (S.H.R.)), the Tobacco-Related Disease Research Program (HIPRA 29IP-0597) (B.N.G.), National Institutes of Health (NIH) grant R01CA208303 (B.N.G.), the National Heart, Lung, and Blood Institute (PO1 HL108793) (B.R.S.), NIH grant DK065988 (S.H.R.), a grant from the W. M. Keck Foundation (B.N.G.) and a grant from Celgene/BMS (B.R.S.). J.L. was supported by the UCLA Tumor Cell Biology Training Program (USHHS Ruth L. Kirschstein Institutional National Research Service Award T32 CA009056). S.S. was supported by the UCLA Broad Stem Cell Research Center–Rose Hills Foundation Training Award and, currently, the UCLA Dissertation Year Fellowship. K.P. and B.N.G. were supported by the UCLA Broad Stem Cell Research Center, the David Geffen School of Medicine and the Jonsson Comprehensive Cancer Center, and K.P. was supported by the NIH (P01 GM099134). The research of K.P. was also supported, in part, by a Faculty Scholar grant from the Howard Hughes Medical Institute. J.E. was funded by the NIH (DP1DA044371), and J.E. and B.N.G. were supported by the Jonsson Comprehensive Cancer Center and the Eli and Edythe Broad Center of Regenerative Medicine and Stem Cell Research Ablon Scholars Award. C.J.A. and D.W.S. were supported by a UCLA Medical Scientist Training Program grant (NIH NIGMS GM008042), the NIH/NCI NRSA Predoctoral F31 Diversity Fellowship F31CA239655 (C.J.A.), the Eli and Edythe Broad Center of Regenerative Medicine and Stem Cell Research Training Grant (C.J.A.), the T32 National Research Service Award in Tumor Cell Biology CA009056 (C.J.A.), the Parker B. Francis Foundation Fellowship (C.Y.) and UCLA CTSI KL2- NCATS KL2TR001882 (C.Y.).

## Author contributions

A.L.R. was previously known as Amy L. Firth. G.C., J.L. and J.M. designed and performed experiments, analyzed the data and prepared the manuscript. S.S., Z.L., A.P., G.Z., B.K., C.J.A., B.A.C., P.V., C.Y., D.W.S., E.I., T.M.R., E.W., A.S., M.M., A.L. and J.L. assisted in tissue handling, sampling, processing and sorting for scRNA-seq cell culture. J.E. supervised J.L. and S.S. S.H.R., E.K.V., A.L.R. and M.M. provided expertise and/or tissue analysis. K.P., J.M., B.R.S. and B.N.G. supervised the study and prepared the manuscript. All authors reviewed and edited the final manuscript.

## Competing interests

The authors declare no competing interests.

## Additional information

**Extended data** is available for this paper at https://doi.org/10.1038/s41591-021-01332-7.

**Supplementary information** The online version contains supplementary material available at https://doi.org/10.1038/s41591-021-01332-7.

**Correspondence and requests for materials** should be addressed to K.P., J.E.M., B.R.S. or B.N.G.

**Peer review information** *Nature Medicine* thanks Tuomas Tammela, Jeffrey Whitsett, and the other, anonymous reviewers for their contribution to the peer review of this work. Editor recognition statement: Jerome Staal was the primary editor on this article and managed its editorial process and peer review in collaboration with the rest of the editorial team

**Reprints and permissions information** is available at www.nature.com/reprints.

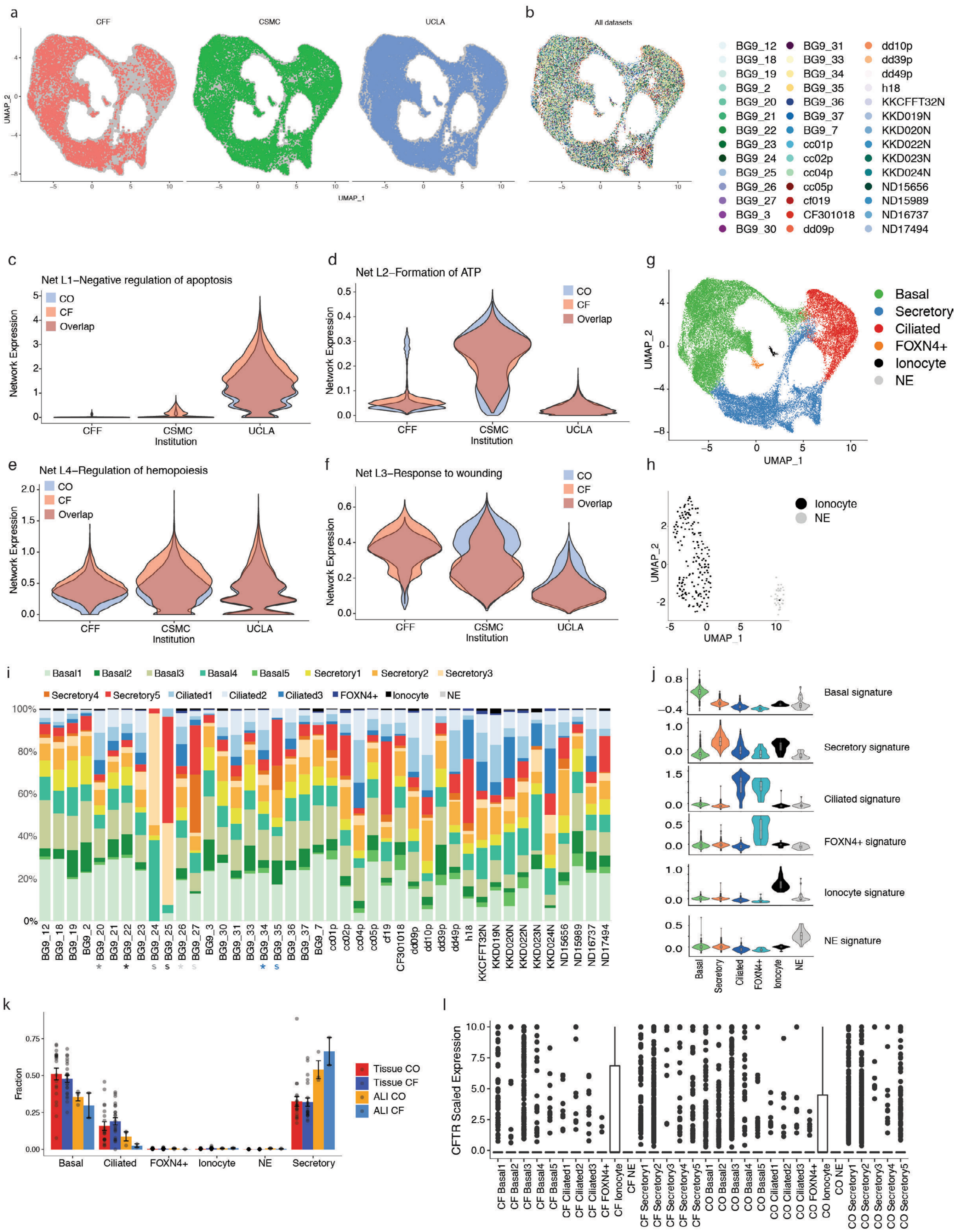

**Extended Data Fig. 1 | See next page for caption.**

**Extended Data Fig. 1 | Cell subsets identified across institutions.** **a**, Visualization of the distribution of cells from the three institutions in the integrated embedding, showed by institution and (b) by samples of origin, visualized by UMAP. **c–f**, Network distributions with differences between institutions, visualized by UMAP. **g**, Major cell types identified using previously described markers, visualized by UMAP. **h**, Ionocyte and NE cell subsets analyzed independently of other cell types, visualized by UMAP. **i**, CO and CF sample contribution to cell populations and subsets, visualized by a stacked column chart. The 's' indicates submucosal gland samples derived from matching '*' CO and CF lungs. **j**, Signatures of major cell types in 10706 ALI cells, created using previously published ALI gene lists, shown by violin plots. Overlaid are boxplots showing the quartiles, whiskers showing 1.5 times interquartile range, and dots showing outliers. **k**, Distribution of major cell type proportions in freshly isolated and ALI datasets, for 38 and 5 independent biological samples respectively. Error bars show the standard error of the mean. **l**, CFTR expression level per subtype, scaled over all cells.

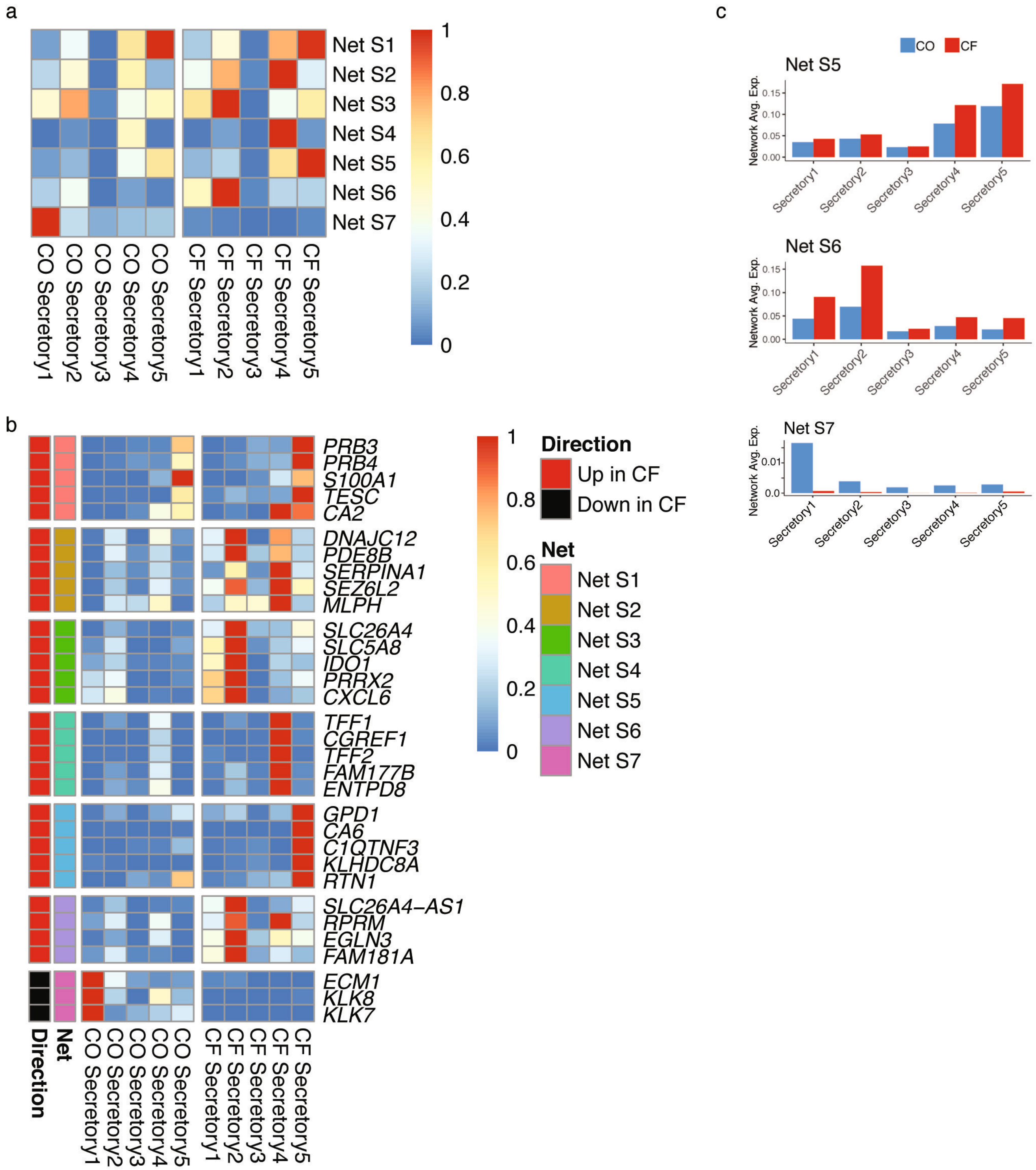

**Extended Data Fig. 2. | Secretory cell networks. a**, Heatmap showing the percent of normalized expression of the seven secretory networks across the secretory subset groups, divided by CO and CF. Each cell shows the average expression of all cells in that category, normalized by row. **b**, Heatmap showing the percent of normalized expression within the secretory subset groups for the top five genes selected from each secretory network based on their pan-institutional identity as either the most Up or Down in CF within the given network. Up/Down and Network classification is shown by annotation to left of heatmap and in key at right. Note for Net S7, only three genes qualified as pan-institutional. **c**, Bar plots showing the average expression of all genes in the remaining individual secretory networks per secretory subset group, in CO or CF cells.

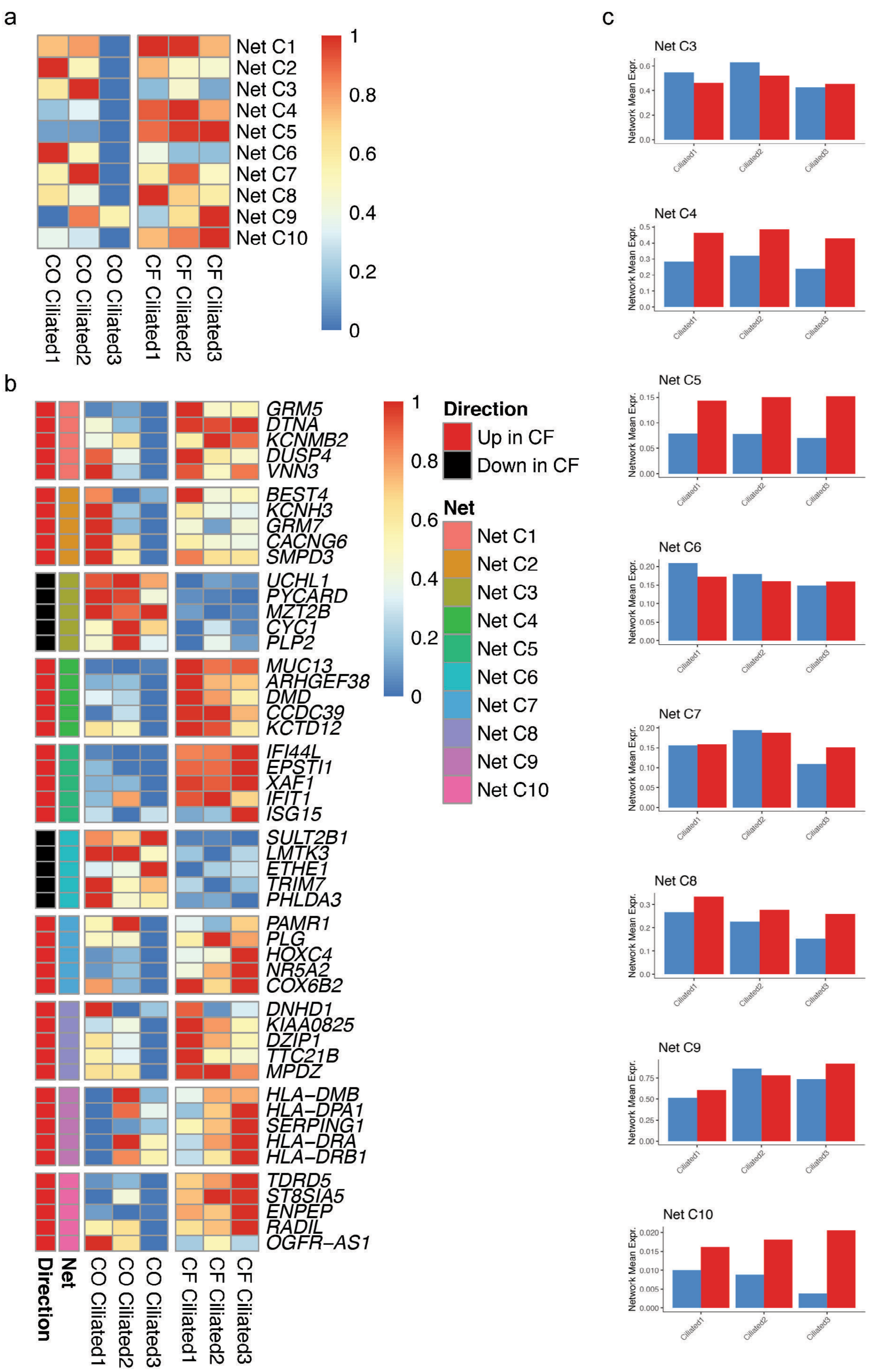

**Extended Data Fig. 3 | See next page for caption.**

**Extended Data Fig. 3 | Ciliated cell networks.** **a**, Heatmap showing the percent of normalized expression of all ten ciliated networks across the ciliated subset groups, divided by CO and CF. Each cell shows the average expression of all cells in that category, normalized by row. **b**, Heatmap showing the percent of normalized expression within the ciliated subset groups for the top five genes selected from each ciliated network based on their pan-institutional identity as either the most Up or Down in CF within the given network. Up/Down and Network classification is shown by annotation to left of heatmap and in key at right. **c**, Bar plots showing the average expression of all genes in the remaining individual ciliated networks per ciliated subset group, in CO or CF cells.

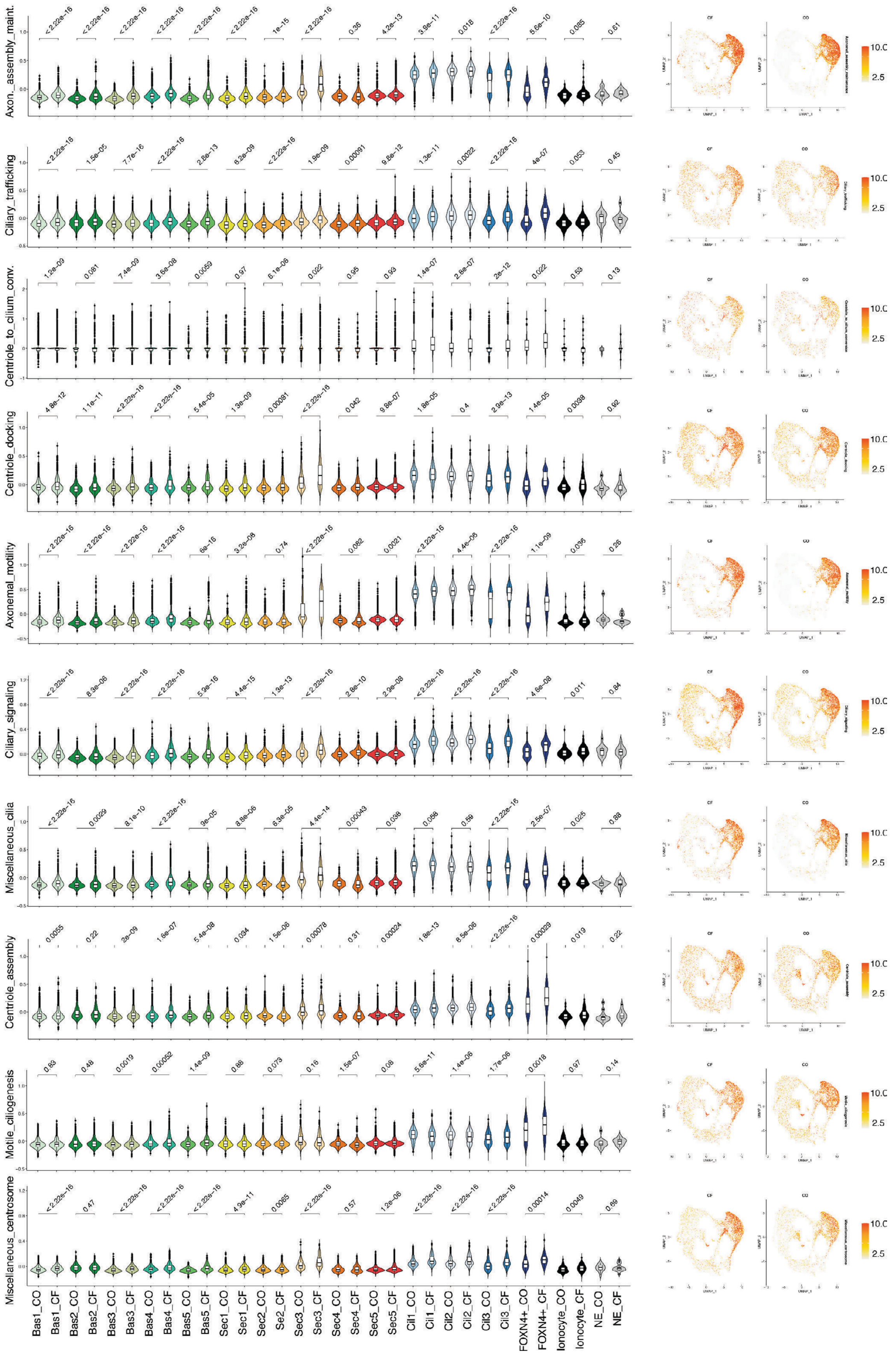

**Extended Data Fig. 4 | Changes in CO and CF cilia biogenesis. a–j**, For distinct categories of genes related to cilia biogenesis, the expansion of cilia gene expression is shown by violin plots and UMAP, indicating the changes in CO and CF for each cell subset. Overlaid are boxplots showing the quartiles, whiskers showing 1.5 times interquartile range, and dots showing outliers. Each Pair of CO and CF show the associated P value (Wilcox test).

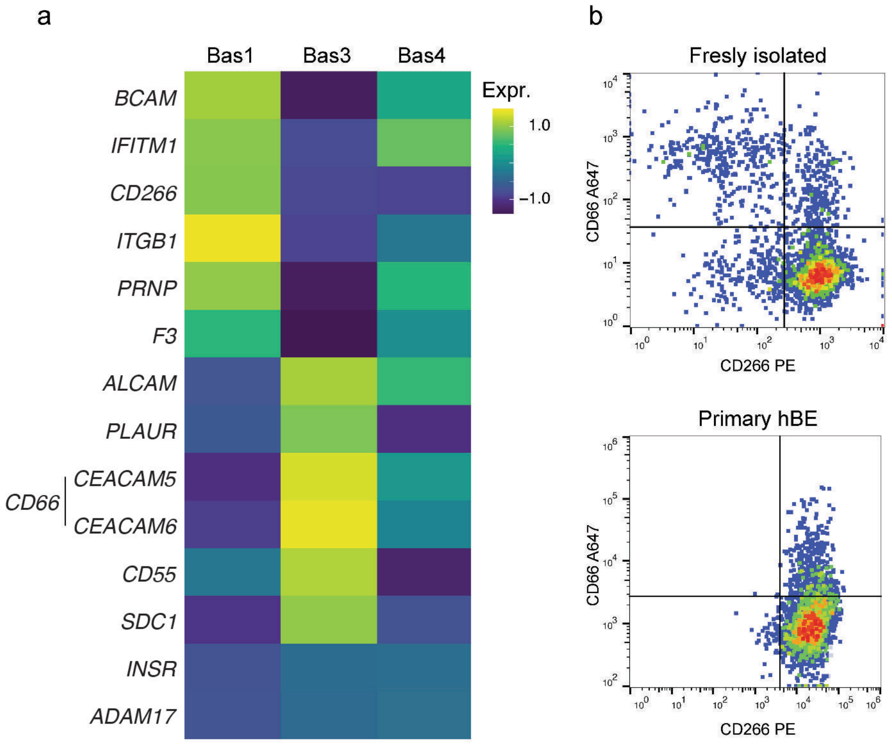

**Extended Data Fig. 5 | Surface markers of basal cell subsets.** **a**, Scaled expression of the top differentially expressed CD marker genes that inform specific basal cell subsets, visualized by heatmap. **b**, FACS plots showing segregation of total basal cells (CD326+, CD271+, CD45-, CD31–) into basal subsets based on their preferential expression of CD66 and CD266, in freshly isolated CO (upper panel) and primary hBE culture (lower panel).

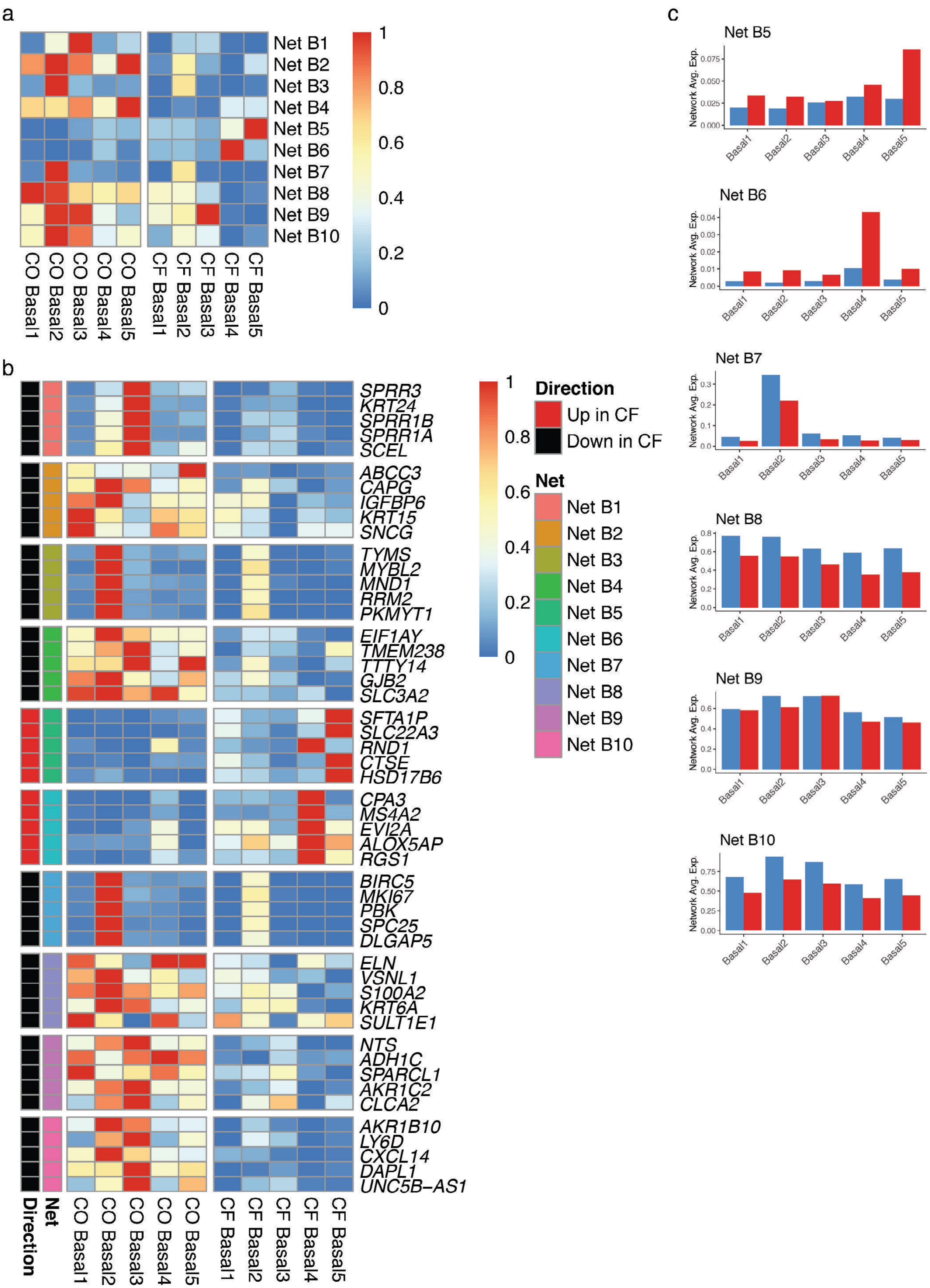

**Extended Data Fig. 6 | See next page for caption.**

**Extended Data Fig. 6 | Basal cell networks. a**, Heatmap showing the percent of normalized expression of the ten basal networks across the basal subset groups, divided by CO and CF. Each cell shows the average expression of all cells in that category, normalized by row. **b**, Heatmap showing the percent of normalized expression within the basal subset groups for the top five genes selected from each basal network based on their pan-institutional identity as either the most Up or Down in CF within the given network. Up/Down and Network classification is shown by annotation to left of heatmap and in key at right **c**, Bar plots showing the average expression of all genes in the remaining individual basal networks per basal subset group, in CO or CF cells.

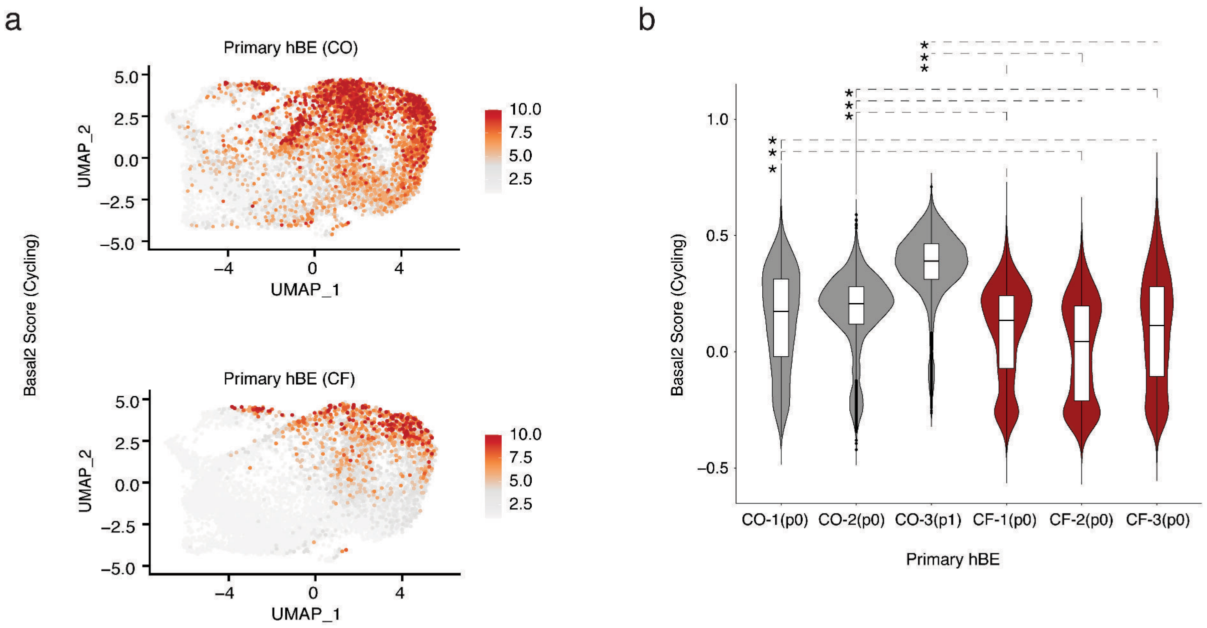

**Extended Data Fig. 7. | Proliferative basal cells in CO and CF. a**, Scoring of the proliferative state (generated using a gene signature from Basal2 subset, Supplementary Table 2), of primary hBE from CO and CF, visualized by UMAP. **b**, Same scoring showed as violin plots with pairwise t-test comparison of CO and CF, *: $p < 2.22e-16$ (Wilcox test). Overlaid are boxplots showing the quartiles, whiskers showing 1.5 times interquartile range, and dots showing outliers. 3 clones were sampled for each condition.

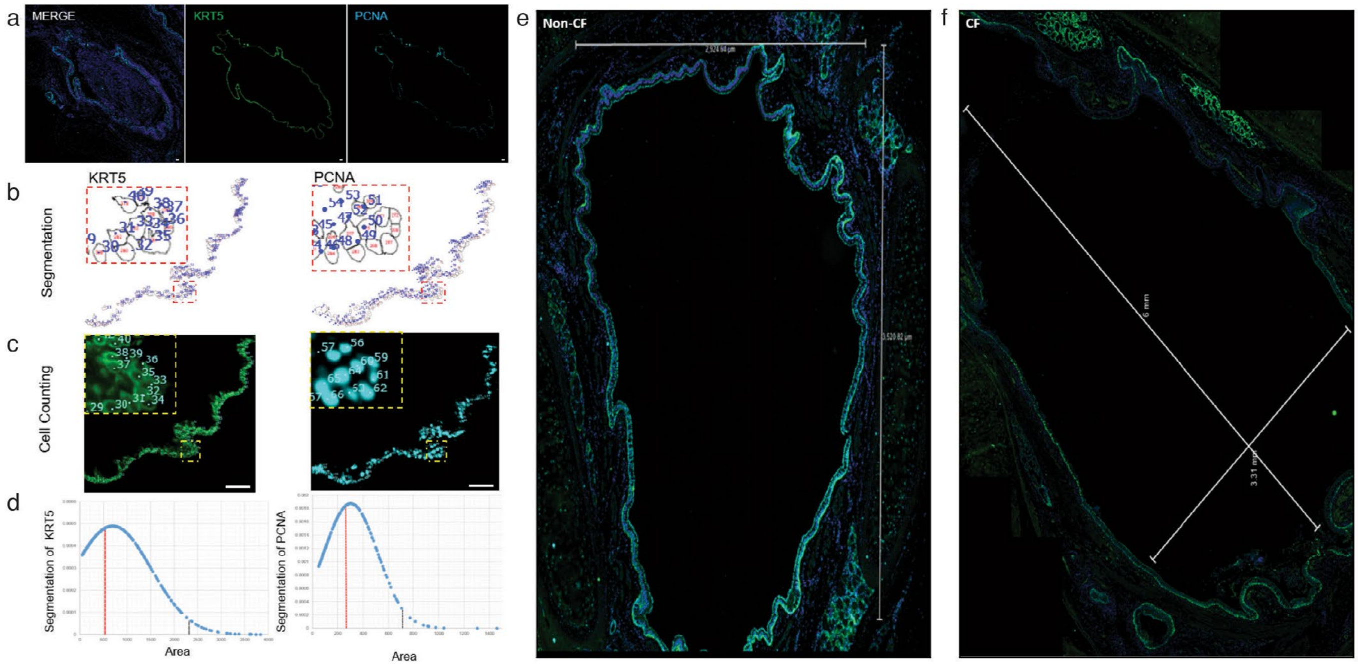

**Extended Data Fig. 8 | Counting proliferative basal cell in CO and CF.** **a**, Representative IF images of airways showing KRT5 (green) and PCNA (cyan), all nuclei are counterstained with DAPI (blue) in the merged image. Scale bar shows 75 µm. **b**, Representative examples of watershed segmentation for isolated KRT5 and PCNA staining. **c**, Representative images indicating counting of KRT5 (green) and PCNA (cyan) expressing cells in the segmented images. Scale bar shows 75 µm. Red and yellow boxes highlight areas that provide 4x zoomed images. **d**, Segmentation data assumes a normal distribution. Each data point represents a possible cell and its corresponding area. Red line represents the mean area of the data and black line represents two standard deviations above the mean area. Representative tiles scan regions taken at 20x magnification for non-CF (e) and CF (f) subjects stained for KRT5 (green), PCNA (cyan) and nuclei are counterstained with DAPI (blue). Dimensions of the airways are indicated by the white lines. In all cases, images are representative of 14 CF and 17 CO fields of view.

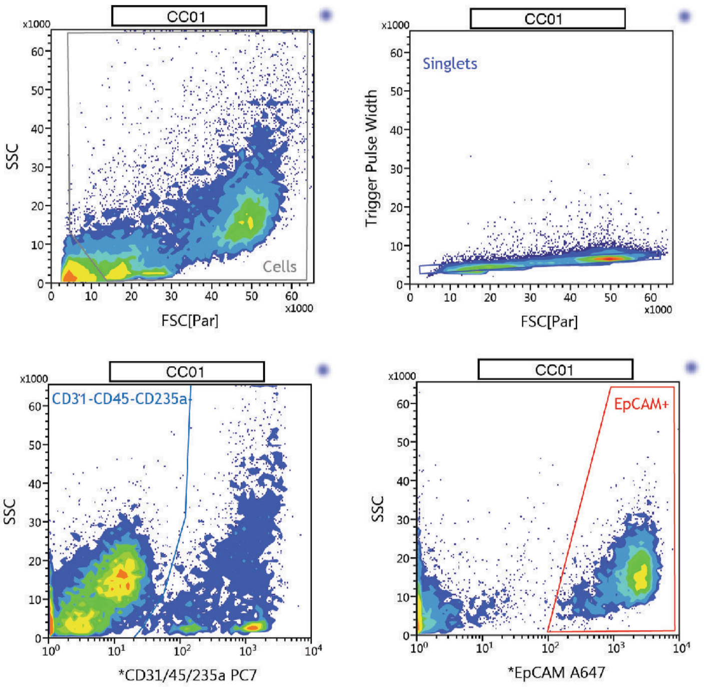

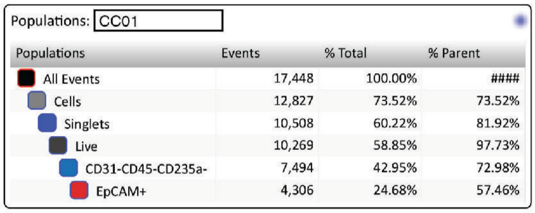
Populations: CC01

| Populations | Events | % Total | % Parent |
|---|---|---|---|
| ⬛ All Events | 17,448 | 100.00% | #### |
| ■ Cells | 12,827 | 73.52% | 73.52% |
| 🟦 Singlets | 10,508 | 60.22% | 81.92% |
| ⬛ Live | 10,269 | 58.85% | 97.73% |
| 🟦 CD31-CD45-CD235a- | 7,494 | 42.95% | 72.98% |
| 🟥 EpCAM+ | 4,306 | 24.68% | 57.46% |

**Extended Data Fig. 9 | FACs isolation of airway epithelial cells.** Representative FACS plots for isolation of epithelial cells to use in scRNAseq with 10X Genomics. Cell debris were excluded on the basis of FSC-A versus SSC-A, then doublets were removed using Trigger Pulse Width versus FSC-A (Influx). Dead cells were identified and excluded on the base of staining with DAPI. Negative gating for CD45, CD31, and CD235a, combined with positive gating for EPCAM (CD326) were used to identify epithelial cells.

nature research

Corresponding author(s): Brigitte N. Gomperts<br>
Barry R. Stripp<br>
John Mahoney<br>
Kathrin Plath

Last updated by author(s): Mar 8, 2021

# Reporting Summary

Nature Research wishes to improve the reproducibility of the work that we publish. This form provides structure for consistency and transparency in reporting. For further information on Nature Research policies, see Authors & Referees and the Editorial Policy Checklist.

## Statistics

For all statistical analyses, confirm that the following items are present in the figure legend, table legend, main text, or Methods section.

| n/a | Confirmed | |
|---|---|---|
| □ | ☒ | The exact sample size (*n*) for each experimental group/condition, given as a discrete number and unit of measurement |
| □ | ☒ | A statement on whether measurements were taken from distinct samples or whether the same sample was measured repeatedly |
| □ | ☒ | The statistical test(s) used AND whether they are one- or two-sided<br>*Only common tests should be described solely by name; describe more complex techniques in the Methods section.* |
| □ | ☒ | A description of all covariates tested |
| □ | ☒ | A description of any assumptions or corrections, such as tests of normality and adjustment for multiple comparisons |
| □ | ☒ | A full description of the statistical parameters including central tendency (e.g. means) or other basic estimates (e.g. regression coefficient) AND variation (e.g. standard deviation) or associated estimates of uncertainty (e.g. confidence intervals) |
| □ | ☒ | For null hypothesis testing, the test statistic (e.g. *F*, *t*, *r*) with confidence intervals, effect sizes, degrees of freedom and *P* value noted<br>*Give P values as exact values whenever suitable.* |
| ☒ | □ | For Bayesian analysis, information on the choice of priors and Markov chain Monte Carlo settings |
| □ | ☒ | For hierarchical and complex designs, identification of the appropriate level for tests and full reporting of outcomes |
| □ | ☒ | Estimates of effect sizes (e.g. Cohen's *d*, Pearson's *r*), indicating how they were calculated |

*Our web collection on statistics for biologists contains articles on many of the points above.*

## Software and code

Policy information about availability of computer code

| | |
|---|---|
| Data collection | For imaging:<br>Immunofluorescence were created using Leica's LAS X 3.4.2.18368 or Zeiss's Zen Blue 2.3 softwares.<br>For scRNAseq data:<br>At CSMC and CFF, Cell Ranger software was used for mapping and barcode filtering. The raw reads were aligned to the transcriptome using STAR, using a hg38 transcriptome reference from GENCODE 25 annotation. Expression counts for each gene in all samples were collapsed and normalized to unique molecular identifier (UMI) counts. The result is a large digital expression matrix with cell barcodes as rows and gene identities as columns. At UCLA, raw sequencing data were filtered by read quality, adapter- and polyA-trimmed, and reads satisfying a length threshold of 30 nucleotides were aligned to the human genome using Bowtie2. Aligned reads were tagged to gene exons using Bedtools Intersect. DGE matrices were then generated by counting gene transcripts for all cells within each sample using custom Python scripts. Cell barcodes were merged within 1 Hamming distance. |
| Data analysis | For imaging:<br>Images were cleaned using Photoshop 21.2.5 (Adobe Inc., San Jose, CA) by creating a masking layer to select for expressing cells and from this mask, overlapping co-expressing cells were isolated. These images were then converted to 8-bit and analyzed on Fiji 2.1.0 (Schindelin et al. 2012) by setting appropriate thresholds, creating a binary mask, and performing a watershed segmentation (Supplemental Fig. SXB). These segmented images were then measured, and actual counts were obtained using a minimum area of 100 and a maximum area of two standard deviations above the mean area of pixels. The basal cell proliferative index was obtained by dividing the number of isolated PCNA-immunoreactive nuclei by the total number of KRT5-immunoreactive cells. For in-situ hybridization experiments, images were processed in a similar way using Fiji. All data were compared using an unpaired student's t-test; results were considered significant when p<0.05.<br>For scRNAseq data:<br>Data analysis was mainly performed with Seurat 3.0. Quality control and filtering were performed to remove cells with low number of expressed genes (threshold n>=200) and elevated expression of apoptotic transcripts (threshold mitochondrial genes < 15%). Only genes detected in at least 3 cells were included. Each dataset was run with SoupX analysis package 1.3.6 to remove contaminant 'ambient' RNA derived from lysed cells during isolation and capture. To minimize doublet contamination for each dataset we performed a quantile |

thresholding of high UMI using a fit model generated using the multiplet's rate to recovered cells proportion. The raw expression matrix was processed with SCTransform 0.3.2 wrapper in Seurat. Clustering was performed with the R implementation of the Leiden algorithm 0.3.7. Differential gene expression was performed with MAST 1.16.0 within Seurat's FindMarkers function.

For manuscripts utilizing custom algorithms or software that are central to the research but not yet described in published literature, software must be made available to editors/reviewers. We strongly encourage code deposition in a community repository (e.g. GitHub). See the Nature Research guidelines for submitting code & software for further information.

## Data

Policy information about availability of data

All manuscripts must include a data availability statement. This statement should provide the following information, where applicable:

- Accession codes, unique identifiers, or web links for publicly available datasets
- A list of figures that have associated raw data
- A description of any restrictions on data availability

Sequence data that support the findings of this study have been deposited in the NCBI GEO "GenBank" with the accession code GSE150674.
All requests for raw and analyzed data and materials will be promptly reviewed by Brigitte Gomperts to verify whether the request is subject to any intellectual property.

# Field-specific reporting

Please select the one below that is the best fit for your research. If you are not sure, read the appropriate sections before making your selection.

☒ Life sciences □ Behavioural & social sciences □ Ecological, evolutionary & environmental sciences

For a reference copy of the document with all sections, see nature.com/documents/nr-reporting-summary-flat.pdf

# Life sciences study design

All studies must disclose on these points even when the disclosure is negative.

Sample size

For scRNAseq:
Proximal airway epithelium isolated from lung tissue from patients with no evidence of chronic lung diseases (CO) (n=19) was compared to patients undergoing transplantation for end-stage CF lung disease (n=19).
For image analysis of immunofluorescence and in situ hybridization CO and CF had n from a minimum of 3 to a maximum of 6.

Data exclusions

For all scRNAseq data, quality control and filtering were performed to remove cells with low number of expressed genes (threshold n>=200) and elevated expression of apoptotic transcripts (threshold mitochondrial genes < 15%). Exclusion criteria were pre-established.

Replication

scRNAseq data were independently produced in three institutions. No additional experiments other than the experiments reported here, were performed. After initial quality control and filtering, datasets from the three institutions were integrated into the same manifold, that was used for all subsequent analyses. Distribution of cells from the three institutions in the manifold, showed homogeneous data integration and proper compensation of batch effects.

Randomization

Samples were allocated in two major experimental groups, Control and Cystic Fibrosis. The samples are representative of the two populations of interest. Samples were recruited on the base of availability and it is not possible to guarantee their similarity with respect to known covariates.

Blinding

Investigators were blinded to group allocation during analysis of staining.

# Reporting for specific materials, systems and methods

We require information from authors about some types of materials, experimental systems and methods used in many studies. Here, indicate whether each material, system or method listed is relevant to your study. If you are not sure if a list item applies to your research, read the appropriate section before selecting a response.

## Materials & experimental systems

| n/a | Involved in the study |
|---|---|
| ☐ | ☒ Antibodies |
| ☒ | ☐ Eukaryotic cell lines |
| ☒ | ☐ Palaeontology |
| ☒ | ☐ Animals and other organisms |
| ☐ | ☒ Human research participants |
| ☒ | ☐ Clinical data |

## Methods

| n/a | Involved in the study |
|---|---|
| ☒ | ☐ ChIP-seq |
| ☐ | ☒ Flow cytometry |
| ☒ | ☐ MRI-based neuroimaging |

# Antibodies

Antibodies used

For imaging:
PCNA (Cell Signaling Technology, #13110), KRT5 (Biolegend, #905901), SCGB1A1 (R&D, MAB4218), FOXJ1, MUC5AC, LTF (Thermo Fisher, 14-9965-82, MA5-12175, PA5-19036), MUC5B (Sigma, HPA008246), TP63 (Cell Signaling, D2K8X), KRT5 (Biolegend, Poly9059), BPIFA1 (R&D, AF1897), TUBA4A (Sigma, T7471).
For FACS:
EPCAM (Biolegend, #369820), CD235a (Biolegend, 349106), CD45 (Biolegend,368522), and CD31 (Biolegend,303124)
To evaluate basal cell subsets, freshly isolated or ALI day 0 cells were stained with PE-Cy7 anti-human CD31 and CD45 (Biolegend, 303117, 368531), AF488 anti-human CD326 (Biolegend, 324209), PerCP-Cy5.5 anti-human CD271 (Biolegend, 345111), AF647 anti-human CD66 (Biolegend, 342307), PE anti-human CD266 (Biolegend, 314004).

Validation

Each antibody was selected from Biolegend antibodies and tested for flow cytometry with human samples.
The specificity of primary antibodies was validated by staining against lgG controls.

# Human research participants

Policy information about studies involving human research participants

Population characteristics

CF tissue was obtained from donors with end stage disease undergoing transplantation. Control tissue was obtained from lungs unsuitable for transplantation. No organs/tissues were procured from prisoners.

Recruitment

Human lung tissue was obtained from Cedars-Sinai Medical Center (CSMC), the University of North Carolina at Chapel Hill (UNC) CF Center Tissue Procurement and Cell Culture Core, University of Texas Southwestern (UTSW), University of California Los Angeles (UCLA), University of Southern California (USC), and the University of Iowa. CF tissue was obtained from donors with end stage disease undergoing transplantation, while human lungs unsuitable for transplantation were obtained from Carolina Donor Services (Durham, NC), the National Disease Research Interchange (Philadelphia, PA), or the International Institute for Advancement of Medicine (Edison, NJ).

Ethics oversight

Human lung tissues were procured under each institutions approved IRB protocols #00035396 (CSMC), #03-1396 (UNC), # 1172286 (CFF and WCG-Copernicus Group WIRB) and #16-000742 (UCLA). Informed consent was obtained from lung donors or authorized representatives.

Note that full information on the approval of the study protocol must also be provided in the manuscript.

# Flow Cytometry

## Plots

Confirm that:

☒ The axis labels state the marker and fluorochrome used (e.g. CD4-FITC).

☒ The axis scales are clearly visible. Include numbers along axes only for bottom left plot of group (a 'group' is an analysis of identical markers).

☒ All plots are contour plots with outliers or pseudocolor plots.

☒ A numerical value for number of cells or percentage (with statistics) is provided.

## Methodology

Sample preparation

Tissue was enzymatically digested with Liberase followed by gentle scraping of epithelial cells off the basement membrane. Tissue was finely minced and washed in Ham's F12 (Corning) at 4°C for 5 minutes with rocking, followed by centrifugation for 5 minutes at 600g and 4°C. The minced cleaned tissue was then incubated in DMEM/F12 (Thermo Fisher Scientific) containing 1X Liberase (Sigma-Aldrich), incubated at 37°C with rocking for 45 minutes. Dissociated single-cell preparations were enriched for epithelial cells and depleted of erythrocytes, leukocytes, and endothelial cells using antibodies with dilution 1:200, against the following molecules: EPCAM (CO17-1A, 369820), CD235a (HI264, 349106), CD45 (2D1,368522), and CD31 (WM59,303124) (Biolegend). Labeled cells were washed in HBSS with 2% FBS, resuspended and placed on ice for fluorescence-activated cell sorting (FACS) using a BD Influx cell sorter (Becton Dickinson). Viability was determined by staining cell preparations with DAPI (ThermoFisher Scientific), 15 minutes prior to cell sorting.

| | |
|---|---|
| Instrument | BD Influx cell sorter (Becton Dickinson, BD) or a Sony SH800S for ALI cells. |
| Software | BD FACS Sortware software 1.2.0.142 for BD Influx, and Cell Sorter Software 2.1.5 for Sony SH800S. |
| Cell population abundance | A small aliquot of sorted epithelial cells were rerun on the BD Influx cell sorter using the same settings as the initial sort. This post-sort flow cytometric analysis revealed a purity of greater than 98%. |
| Gating strategy | Cell debris was first discarded on the basis of FSC-A and SSC-A, and doublets were removed using FSC-A and trigger pulse width. Dead cells were identified and removed on the basis of staining with DAPI. Negative gating for (CD45-, CD31 , CD235a-) and positive gating for (EPCAM) were used to enrich epithelial cells. |

☒ Tick this box to confirm that a figure exemplifying the gating strategy is provided in the Supplementary Information.